LEVEL III

(10)

A048483
SR#2

(19) RADC-TR-78-115
Interim Report
May 1978

(12) 104p.

(6) STUDY OF THE PHYSICS OF INSULATING FILMS AS RELATED TO THE RELIABILITY OF METAL-OXIDE SEMICONDUCTOR DEVICES

(10) D. R. Young,
E. A. Irene,
D. W. Dong,
D. J. DiMaria
R. F. DeKeersmaecker
Z. A. Weinberg
G. Rubloff
W. R. Hunter
C. M. Serrano

IBM T. J. Watson Research Center

Sponsored by
Defense Advanced Research Projects Agency (DoD)
ARPA Order No. 2180

(14) SCIENTIFIC-3

Approved for public release; distribution unlimited.

(9) Interim rept. 17 May - 16 Nov 77,

(15) F19628-76-C-0249, ARPA Order-2180

ROME AIR DEVELOPMENT CENTER
Air Force Systems Command
Griffiss Air Force Base, New York 13441

(16) 2306, 2180 (17) J3

This report has been reviewed by the RADC Information Office (OI) and is releasable to the National Technical Information Service (NTIS). At NTIS it will be releasable to the general public, including foreign nations.

RADC-TR-78-115 has been reviewed and is approved for publication.

APPROVED: John C. Garth

JOHN C. GARTH
Project Engineer

If your address has changed or if you wish to be removed from the RADC mailing list, or if the addressee is no longer employed by your organization, please notify RADC (ESR), Hanscom AFB MA 01730. This will assist us in maintaining a current mailing list.

Do not return this copy. Retain or destroy.

UNCLASSIFIED

SECURITY CLASSIFICATION OF THIS PAGE (When Data Entered)

REPORT DOCUMENTATION PAGE

READ INSTRUCTIONS BEFORE COMPLETING FORM

1. REPORT NUMBER: RADC-TR-78-115	2. GOVT ACCESSION NO.
3. RECIPIENT'S CATALOG NUMBER	
4. TITLE (and Subtitle): STUDY OF THE PHYSICS OF INSULATING FILMS AS RELATED TO THE RELIABILITY OF METAL-OXIDE SEMICONDUCTOR DEVICES	5. TYPE OF REPORT & PERIOD COVERED: Interim Report 17 May 77 - 16 Nov 77
	6. PERFORMING ORG. REPORT NUMBER: Scientific Report #3
7. AUTHOR(s): D. R. Young, D. J. DiMaria, G. Rubloff, E. A. Irene, R. F. DeKeersmaecker, W. R. Hunter, D. W. Dong, Z. A. Weinberg, C. M. Serrano	8. CONTRACT OR GRANT NUMBER(s): F19628-76-C-0249
9. PERFORMING ORGANIZATION NAME AND ADDRESS: IBM T. J. Watson Research Center, P. O. Box 218, Yorktown Heights NY 10598	10. PROGRAM ELEMENT, PROJECT, TASK AREA & WORK UNIT NUMBERS: 61101E 2180ARAE
11. CONTROLLING OFFICE NAME AND ADDRESS: Advanced Research Projects Agency, 1400 Wilson Blvd, Arlington VA 22209	12. REPORT DATE: May 1978
	13. NUMBER OF PAGES
14. MONITORING AGENCY NAME & ADDRESS(if different from Controlling Office): Deputy for Electronic Technology (RADC/ESR), Hanscom AFB MA 01730, Monitor/John C. Garth/ESR	15. SECURITY CLASS. (of this report): UNCLASSIFIED
	15a. DECLASSIFICATION/DOWNGRADING SCHEDULE: N/A

16. DISTRIBUTION STATEMENT (of this Report)

Approved for public release; distribution unlimited.

17. DISTRIBUTION STATEMENT (of the abstract entered in Block 20, if different from Report)

Same

18. SUPPLEMENTARY NOTES

RADC Project Engineer:
J. C. Garth (ESR)

Related In-House 2306J301

611 02F

19. KEY WORDS (Continue on reverse side if necessary and identify by block number)

MOS Structures
Si Oxidation
Hole Trapping
Electron Trapping
As Implantation
photo detrapping

20. ABSTRACT (Continue on reverse side if necessary and identify by block number)

The current papers described the oxidation of heavily doped silicon , the location of implanted ions in SiO_2, a light activated storage device (LASD) and exciton model for $Si-SiO_2$ interface state generation and electron trapping and photo detrapping on sites related to As implantation in SiO_2.

DD FORM 1 JAN 73 1473 EDITION OF 1 NOV 65 IS OBSOLETE

UNCLASSIFIED

SECURITY CLASSIFICATION OF THIS PAGE (When Data Entered)

TABLE OF CONTENTS

1.	Introduction	4
2.	Silicon Oxidation Studies: The Oxidation of Heavily B and P Doped Single Crystal Silicon	8
3.	Light Activated Storage Device (LASD)	28
4.	Exciton Creation and Transport in SiO_2 as a Cause of Surface State Generation in SiO_2 Structures	44
5.	Electron Trapping and Detrapping Characteristics of Arsenic Implanted SiO_2 Layers	58
6.	Centroid Location of Implanted Ions in the SiO_2 Layer of MOS Structures using the Photo I-V Technique	91

INTRODUCTION

Our strong emphasis on charge buildup and transport in SiO_2 continues due to the key role this insulator plays in modern integrated circuit technology. These effects are on the one hand intimately related to many important device reliablity problems and on the other hand offer new device opportunities due to the possibilities of using charge stored in the insulator to provide electrical means for changing the device characteristics. We are considering both of these implications in our work.

We have used our automated "insitu" ellipsometer to study the oxidation of heavily B and P doped Si over the temperature range of 780°C - 1150°C. This has provided us with the most complete data covering this wide temperature range. Departures from Arrhenius behavior have shown the reason for the discrepancy in activation energies obtained by earlier workers covering more limited temperature ranges. This paper has been submitted to the Jr. of Electrochem. Soc. and a talk will be given at the Special Symposium on Oxidation at the E.C.S. Meeting in Seattle as follows:

Silicon Oxidation Studies: The Oxidation of Heavily B and P Doped Single Crystal Silicon

E. A. Irene and D. W. Dong

The observation that electrons trapped on sites related to P and As implantation, can be detrapped optically has suggested a new device possibility that we call the LASD (Light Activated Storage Device). The characteristics of this device are described in the following paper that is being submitted for publication.

Light Activated Storage Device (LASD)

D. J. DiMaria, R. F. DeKeersmaecker, and D. R. Young

A paper has been published in App. Phys. Lett. 32, 184, (1978) describing the work that has led us to propose an Exciton Model for the generation of positive charge and interface states at the Si-SiO_2 interface as a result of the application of non-penetrating VUV and a negative gate bias. This paper is entitled:

Exciton Creation and Transport in SiO_2 as a

Cause of Surface State Generation in SiO_2 Structures

Z. A. Weinberg and G. W. Rubloff

A comprehensive study of the nature of the traps resulting from As implantation has been completed. This includes measurements of the trapping parameters (cross section, denisty, location) photo detrapping measurements, and dependence on annealing treatment.

The electron trapping resulting from As implantation yields the largest cross section we have observed to date ($\sim 1 \times 10^{-15} cm^2$). In addition, the electrons trapped on these sites are stable with respect to the application of relatively large electric fields. These results suggest the use of As in device structures that use charge storage but also indicates that As should be avoided in devices where the electron trapping has a deleterious effect.

This will be submitted for publication in the near future as follows:

Electron Trapping and Detrapping Characteristics

of Arsenic Implanted SiO_2 Layers

R. F. DeKeersmaecker and D. J. DiMaria

A summary is enclosed of the results of the use of the photo I-V technique to determine the centroid of implanted ion profiles in SiO_2 covering Al, P and As with energies from 5 to 100 keV. The results of these measurements are compared with the empirical relationship of Chu, Crowder, Mayer and Ziegler.

The title of this paper and authors are:

Centroid Location of Implanted Ions in the SiO_2 Layer of MOS Structures using the Photo I-V Technique

D. J. DiMaria, D. R. Young, R. F. DeKeersmaecker

W. R. Hunter and C. M. Serrano

We are still holding up the publication of our results of P implantation, since we have not been able to resolve the reproducibility problem which is not understood.

RC 6879 (#29493) 12/05/77
Chemistry 11 pages

Silicon Oxidation Studies: The Oxidation of Heavily B and P Doped Single Crystal Silicon

E.A. Irene and D.W. Dong

IBM T.J. Watson Research Center
Yorktown Heights, New York 10598

Typed by Barbara Fiore on CMC (ei.2021)

Abstract

The present oxidation study covers the 780° - 1150°C temperature range using .001 Ω-cm Si which is heavily B and P doped Si ($6\text{-}8\times10^{19}$ cm^{-3}) in dry O_2 (< 1ppm H_2O). Emphasis is on the lower temperatures thereby extending the scope of already published studies. For .001 Ω-cm Si at temperatures greater than 1000°C, the overall oxidation rates were found to conform to the order:

B doped > P doped > STD

(where STD is 2 Ω-cm B doped Si), which is in agreement with published results for the higher temperatures. However, for the lower oxidation temperatures of the present study (≤1000°C) the order for the overall oxidation rates was found to be:

P doped > B doped ≥ STD.

The oxidation data was taken using an automated ellipsometer "in situ" and was analyzed using a linear-parabolic oxidation model. The resulting linear rate constants could be correlated with well known B depletion and P accumulation effects near the Si-SiO_2 interface while a consideration of the structural roles of B and P in the SiO_2 network was necessary to explain the parabolic rate constants. Phase separation of B_2O_3 occurred in the SiO_2 grown on B doped Si and Si percipitation was observed in all the oxides grown at 1150°C but neither of these phenomena are believed to affect the oxidation kinetics. The extended temperature range showed non-Arrhenius behavior which could explain the divergent activation energies reported from published studies.

LIMITED DISTRIBUTION NOTICE

This report has been submitted for publication elsewhere and has been issued as a Research Report for early dissemination of its contents. As a courtesy to the intended publisher, it should not be widely distributed until after the date of outside publication.

Copies may be requested from:
IBM Thomas J. Watson Research Center
Post Office Box 218
Yorktown Heights, New York 10598

Introduction

An understanding of the oxidation kinetics for single crystal silicon which has been heavily doped ($\sim 10^{20}$ cm^{-3}) with donor or acceptor impurities is important in the practice of planar technology. Previous studies on this topic (1-5) have shown that a redistribution of the electrically active impurities (As, B, P, etc.) occurs during the thermal oxidation of Si. Specifically, it was discovered (3,4) that during oxidation the acceptor impurities (Al, B, Ga and In) depleted near the Si surface while donor impurities (As, P, Sb) piled up at the Si surface. The extent to which the redistribution occurs depends upon the oxidation temperature and ambient (3,4,5). At lower temperatures and in an H_2O containing oxidation ambient, B depletes more and P accumulates more. In order to understand these observations several factors are important. Firstly, the relative solubilities of the impurity in Si and SiO_2 is important with donor impurities usually being relatively more soluble in Si(3). Secondly, the diffusivity of the impurity in SiO_2 is important with B having a slightly larger value than P at lower temperatures (6) but in an H_2O containing ambient the diffusivity of B in SiO_2 increases several orders of magnitude.

By utilizing the linear-parabolic model for Si oxidation (7) in conjunction with the published redistribution effects and the fact that the Si dopants increase the oxidation rate when they affect it at all (5), the kinetics of the oxidation of heavily B and P doped Si can be qualitatively predicted. In the linear-parabolic model, the linear rate constant, k_L, is correlated with the reaction between the Si surface and oxidant, while the parabolic rate constant, k_p, is related to the diffusion of oxidant through the SiO_2 film. Then, it is predicted that at lower oxidation temperatures (<1000°C) where P accumulates and B depletes maximally, an accumulation of P at the Si surface will increase k_L maximally and the depletion of B from the surface should yield a minimal effect on k_L. At higher temperatures, where the B depletion is less, the effect on oxidation of a heavily B doped Si surface on k_L should be observed. In order to predict changes in k_p values, the structural implications of B and P on the SiO_2

network must be assessed (8,9). The role of P in SiO_2 is to substitute for Si in the network. The P in SiO_2 is tetrahedrally surrounded by O atoms similarly to Si in Si-O_4 tetrahedra, except that in the P-O_4 tetrahedra one of the O atoms is doubly bonded to P which precludes that O atom from bridging to an adjacent tetrahedron. A loosening of the SiO_2 network results. The net effect of this loosening on oxidation kinetics would be to increase k_p and it would be more pronounced at lower experimental temperatures where other network loosening mechanisms are minimized (such as thermal expansion and thermal vibration). The substitution of B in the SiO_2 network is difficult in low alkali SiO_2. This is due to the fact that B preferentially forms a three coordinate planar trigonal arrangement of O atoms which is structurally incompatable with the Si-O_4 tetrahedra. Consequently, a study aimed at defining the subliquidus miscibility gap in the SiO_2-B_2O_3 system (10) has shown that phase separation extends to the Si phase boundary with an upper consolute temperature of ~ 520°C. However, the effect of phase separation on the oxidation kinetics would be minimal because the amount of B_2O_3 phase is less than 1 at % and the separation would not occur above 600°C i.e. during oxidation. An alternate mechanism has been proposed (11) in which a large number of oxygen vacancies are created when B cations enter the SiO_2 network. These defects occur as B O_3 is oxidized to B O_4 and are most likely to occur at higher temperatures where themal vibrations create the greatest number of broken bonds. Therefore, the effect of B should be to increase k_p predominantly at high temperatures.

In order to test these predictions of the effect of B and P on k_L and k_p values, the oxidation data already published (5) needs to be extended to cover a broader temperature range, in particular lower temperatures. Also, the data needs to be generated in a well-defined ambient and analyzed according to the linear-parabolic model. For these purposes an automated ellipsometer which can observe oxidation "in situ" (12,13) was used to obtain oxidation data in pure dry O_2 (< 1ppm H_2O) (13,14) over the temperature range 780° to 1040°C and with point by point measurements up to 1150°C. The resulting data were analyzed for k_L and k_p values using a previously developed iterative least squares technique (13). Transmission

electron microscopy (TEM) was used to survey whether any obvious morphological changes could explain the kinetic results.

Experimental Procedures

Wafer Preparation. The B, P and As doped Si slices were commercially acquired 3.2 cm diameter, 0.025 cm thick, <100> oriented chem-mechanically polished Si slices. They were purchased as having a nominal bulk resistivity of 0.0008 - .0012 Ω - cm. Measurements at our laboratory yielded average values of .0016 Ω - cm for B doped and .0009 for P and .0022 for As doped material all values within ± 5% across the wafers. These resistivity values correspond to concentrations of about 6×10^{19} cm^{-3} for B and 8×10^{19} cm^{-3} for P doped material.

Prior to oxidation the wafers were thoroughly cleaned by a previously detailed procedure (14). For transmission electron microscopy observations, 3 mm by 3 mm chips of Si with the SiO_2 film on one side were prepared by a previously outlined procedure (15).

Gas Purity. The moisture content of O_2 and its effect on Si oxidation kinetics has been the subject of several previous studies at our laboratory (13,14,16). The gaseous O_2 used for the present study is from boil-off of liquid oxygen, and has been purified by a previously published procedure[14] which removes hydrocarbons and thereby reduces the H_2O content to less than 1 ppm as measured at the oxidation tube exit under oxidation conditions.

Ellipsometry. The automated ellipsometer which can measure oxide thickness while oxidation is occurring, "in situ", has been described previously (12). The procedures for the use of the automated ellipsometer, temperature calibration, and optical constants used for ellipsometry calculations have also been previously published[12,13]. The analyses of thickness (d) and time (t) data has been done by a linear least squares technique (13). Preliminary ellipsometry measurements made on oxide grown on heavily B and P doped Si have shown that the doping does not alter the optical constants or procedures used for the ellipsometry performed on undoped silicon.

Results and Discussion

Overall Oxidation Rates. From the thickness-time oxidation data presented in Fig. 1a-f, several observations can be made. Firstly, when B and P affect the oxidation rate, both dopants enhance the rate as previously reported (see for example ref. 5). At the higher experimental temperatures (1040° and 1150°C) and for thicker films the heavily B doped Si exhibits a higher overall rate than P doped and lightly doped Si, again in nominal agreement with a previous study (5). However, at lower oxidation temperatures, the heavily P doped Si exhibits the highest overall rate and the heavily B doped Si has about the same rate as lightly doped material. Although, this is not in agreement with published results (5), our results are more extensive at the lower temperatures and the trends in our data are predictable based on published depletion and accumulation effects (3,4,5) as presented below. The crossover in the oxidation rates between the heavily P and B doped Si occurs for the 1040°C oxidation at about 2000 Å. Finally, one experiment using heavily As doped Si displayed the same oxidation behavior as for heavily P doped Si but with a slightly lower overall oxidation rate. In order to gain further insight into the "crossover" behavior between P and B as a function of temperature the linear, k_L and parabolic, k_P rate constants need to be considered.

Rate Constants. The k_L and k_P values are shown in Table 1. The errors associated with the 780° to 1040°C data are less than 10% and are primarily due to the approximate nature of the linear-parabolic model (13). For the 1150°C data the errors are estimated to be larger but less than 20% and the increase is due to larger curve fitting errors with the fewer available data points. In accordance with the predictions made earlier which are directly deduced from previous impurity redistribution studies (3,4,5), the k_L values for B at the lower oxidation temperatures do not show any enhancement effect due to B since B is expected to deplete maximally at these temperatures; P shows an enhancement effect on k_L at all temperatures due to the accumulation effect. Also as predicted, at the highest temperatures of the present study (1150°) where the B depletion effect is minimum, the k_L is considerably higher than for P.

The fact that the overall rate for heavily P doped Si is greater than B for the thinner films even at 1040°C is clearly seen as a k_L effect. For thinner films k_L is dominant and k_L for heavily P doped Si is greater than k_L for heavily B doped Si up to 1040°C. Therefore, the crossover which occurs for larger thicknesses at 1040°C must be a k_P effect. The observation that both heavy B and P doping of Si causes an increase in k_L may be related to the fact that these impurities cause a substantial increase in the total (neutral plus ionized) vacancy concentration in Si (17). An enhanced vacancy concentration at the Si surface increases the number of Si atoms exposed to oxidant (by forming ledges, steps etc.) thereby enhancing the amount of reaction at the surface.

The k_P for heavily P doped Si is clearly greater than the standard at the lower temperatures as predicted. The network loosening attributable to P is lost at high temperatures where thermal vibrations and expansion dominate. However, even larger amounts of P in SiO_2 than in the present study should extend the enhanced k_P to higher temperatures.

In addition to the enhanced k_L for heavily B doped Si at high temperatures due to less B depletion, the k_P for B is also enhanced. This latter effect is consistent with Kang's arguments (11) which are predicated on defect equilibria being shifted toward larger defect concentrations at higher temperatures. The B effect on k_P requires many network bonds to be broken as $B\text{-}O_3$ oxidizes to $B\text{-}O_4$. This can most easily occur at higher temperatures where the network vibrations are largest and simultaneously during interstitial diffusion of oxidant where there exists large forces exerted on the network. The net effect of B on k_P is a large enhancement at temperatures above 1000°C and hence gives rise to the crossover between P and B.

It is also interesting to note the variation of d_o values with temperature. As defined in the present study, d_o represents the upper thickness limit of the initial oxidation regime which does not conform to linear parabolic kinetics (7,13,14). The values of d_o are found using the iterative linear least squares analysis previously described (13). From Table 1 it is seen that d_o values for all the samples increases with temperature in the low temperature regime as

previously reported for lightly doped material (13) but at higher temperatures the d_o values decrease. The smaller values of d_o mean that the oxidation data conform to linear-parabolic kinetics earlier during oxidation. The observation that d_o values go through a maximum near 1000°C suggests a change in oxidation mechanism near this temperature. The values of d_o near 200 Å for higher temperature oxidation data agrees with a previous study (7).

Activation Energies. With k_L and k_P values over an extended temperature range, further insight into the oxidation mechanism may be obtained by interpreting the activation energies calculated according to an Arrhenius equation of the form:

$$k = k_o e^{-Ea/RT}.$$

Fig. 2 shows that neither the linear nor parabolic rate constants obey the above Arrhenius equation. This probably means that both k_L and k_P represent a composite rate constant rather than a kinetically simple step. Therefore, a straightforward interpretation of the E_a values is not possible.

The curvature of the Arrhenius plots suggests that the discrepencies which exist between previous studies (7,13) may be due to the different temperature ranges used. To clarify this situation, E_a values were calculated by least squares analysis of four k_L and k_P values at the lower temperatures (780°, 893°, 980° and 1000°C) and separately using four k_L and k_P values at the highest four temperatures (980°, 1000°, 1040° and 1150°C). These E_a values as well as the literature values are compared in Table 2. Since one study considered mainly higher temperature data (7) and the other lower temperature data (13), the discrepency is clearly due to the non-Arrhenius behavior. Even though one study (7) used <111> Si while the other used <100> Si, it was previously shown (14) that there is less than ± 0.2 eV difference between E_a values for <111> and <100> Si orientations in the same temperature interval.

Transmission Electron Miscroscopy (TEM). Samples of SiO_2 grown on heavily P and B doped Si as well as lightly doped Si at 780°C and 1150°C were compared by TEM. The TEM

investigation was directed at finding microstructure (such as voids or channels) which could account for the differences in diffusion behavior. However, except for two observations relating to the appearances of microphases and described below, there were no differences in the different films resolvable in the present TEM study. As to be discussed, the microphase phenomena cannot explain the kinetic results. Therefore, based on this negative TEM result, it is concluded that the diffusion enhancement caused by P in SiO_2 at lower temperatures and B in SiO_2 at higher temperatures are due to the creation of smaller defects (<20 Å) than resolvable in the present study by TEM and probably involve network defects as hypothesized by Kang (11).

As shown in Fig. 3, certain areas of the SiO_2 films grown on heavily B doped Si at 1150°C and to a lesser extent on 780°C grown SiO_2 displayed an amorphous microphase. Since B_2O_3 is expected to phase separate due to structural incompatibilities (8,9,10), we believe that the microphase is amorphous B_2O_3. As estimated from the micrographs the B_2O_3 phase comprises about 0.5% by volume of the film. However, since the regions of SiO_2 film which displayed phase separation were widely separated, a more realistic estimate would be about 0.05%. If all the B were incorporated in the SiO_2, about 0.3% B_2O_3 would be expected. Considering the large errors in estimating the volumes from micrographs and the possibility of loss of B during oxidation, the agreement is reasonable. Because phase separation in the amorphous B_2O_3 - SiO_2 system occurs upon cooling from the oxidation temperature to about 520°C (the upper consolute temperature), there should be no effect on the oxidation kinetics.

In addition to the B_2O_3 microphase in B containing SiO_2 samples, Si islands were observed in all the SiO_2 films grown at 1150°C and an example is shown in Fig. 4. The distribution is sparse as most areas observed had no Si islands. Selected area diffraction and dark field techniques positively identified the islands as crystalline Si (Fig. 4). Only rarely was the same structure seen for films grown at lower temperatures. The fact that this microstruc-

ture occurs predominantly at the high temperatures suggests that a disproportionation reaction with chemical transport is taking place. A reaction such as:

$$Si\ (s) + SiO_2\ (s) = 2SiO\ (g)$$

goes further to the right at higher temperatures near the Si-SiO_2 interface. The gaseous SiO produced diffuses away from the interface into the SiO_2 film and equilibrates producing Si (s) and SiO_2 (s). At the high temperatures a larger amount of SiO (g) is produced and the Si which comes from SiO, has enough mobility to form islands. Thermochemical calculations have shown that at 1150°C, the partial pressure of SiO (g) is about 10^{-3} atm. That pressure of SiO (g) would provide a pressure of Si (g) of more than 10^{-6} atm at 1150°C. At 1150°C the saturation pressure for Si is about 2×10^{-5} atm. Therefore considering a non-ideal system the conditions for the production of free Si in SiO_2 can occur. However, since this effect was seen for the standard, as well as for B and P doped SiO_2 films at 1150°C, no impurity driven effect on oxidation is attributed to the Si percipitation.

Since this study deals with the oxidation of heavily B and P doped Si, the B_2O_3 phase separation effect and the Si percipitation effect will be discussed at greater depth in a future publication.

Conclusions

From an extension of the oxidation data for heavily B and P doped Si to lower temperatures and an analysis of the data in terms of the linear-parabolic model several conclusions are made:

1) P primarily increases the overall oxidation rate at lower temperatures while B is more effective at the higher oxidation temperatures.

2) The accumulation of P and depletion of B at the Si surface explain the variation of k_L values with temperature.

3) The enhancement effect of P on k_P is due to a loosening of the SiO_2 network. When P substitutes for Si in Si - O_4 tetrahedra, fewer bridging oxygens are provided. The net loosening effect is most pronounced at lower temperatures where other network loosening factors are smaller.

4) The enhancement of k_P due to B is due to the creation of defects when B-O_3 is oxidized to B - O_4. This mechanism is favored at higher temperatures where bonds are more likely to be broken.

5) TEM supports the atomistic arguments to explain the k_P results, since no morphological difference were found in the various oxides which could be correlated with an enhanced diffusion of oxidant.

6) Over the extended temperature range of the present study, the Arrhenius relationship is not obeyed. Hence there is no straightforward interpretation of E_a values. However, divergent results from two previous studies (7,13) are explained based on the curvature of the Arrhenius plots.

Acknowledgements

The Authors gratefully acknowledge helpful discussions with Drs. T. Takamori and J.A. Van Vechten and to Drs. A.B. Fowler, R. Ghez and D.R. Young for reviewing this manuscript and to Dr. J. Blum for the silicon substrate resistivity measurements.

This research was partially supported by the Defense Advanced Research Projects Agency and monitored by the Deputy for Electronic Technology, RADC, under Contract F19628-76-C-0249.

Figure 1 Plots of SiO_2 film thickness, d (Å), versus oxidation time, t (min) for heavily B (X), and P (+) doped Si against lightly doped Si (O) showing every fifth data point at (a) 780°C, (b) 893°C, (c) 980°C (d) 1000°C (e) 1040°C and at 1150°C in (f) all the data is shown.

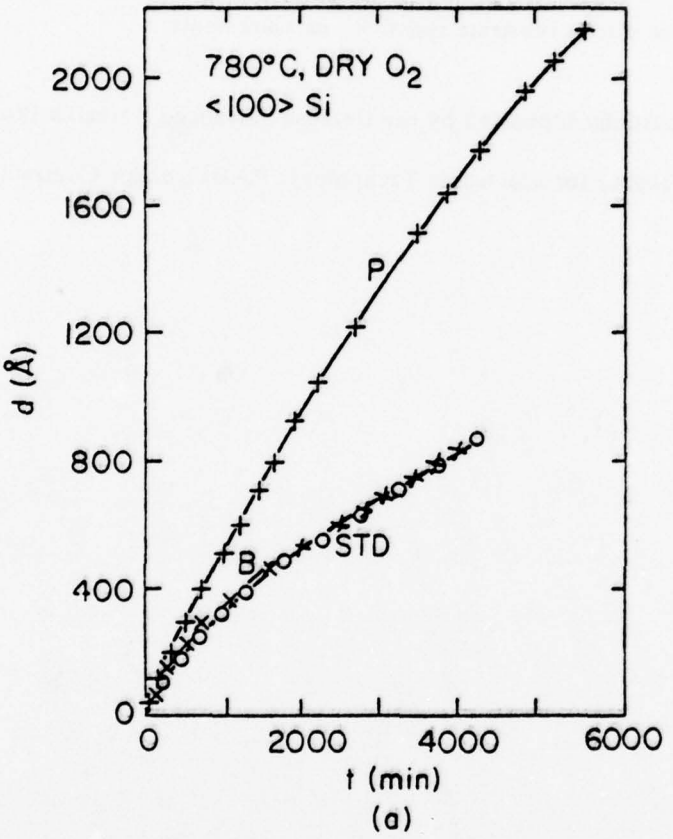

(a)

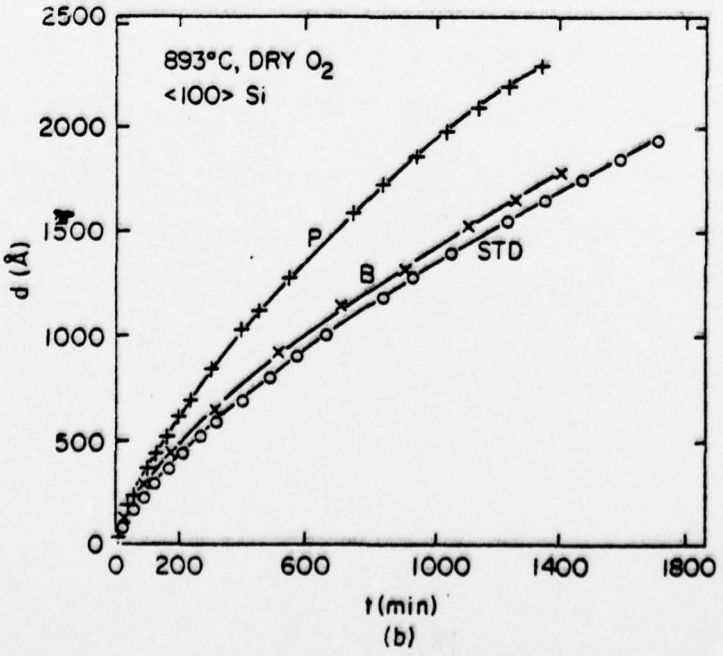

(b)

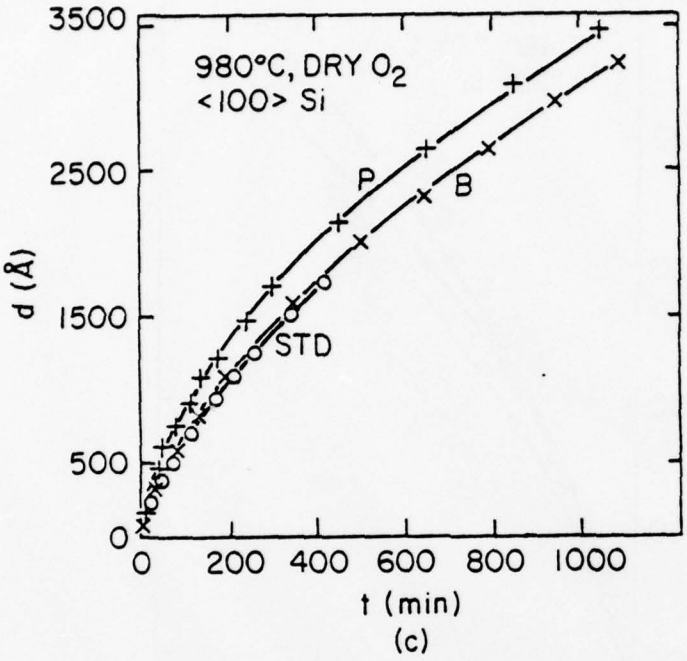
3500
2500
1500
500
0
d (Å)
980°C, DRY O2
<100> Si
P
B
STD
0
200
400
600
800
1000
t (min)
(c)

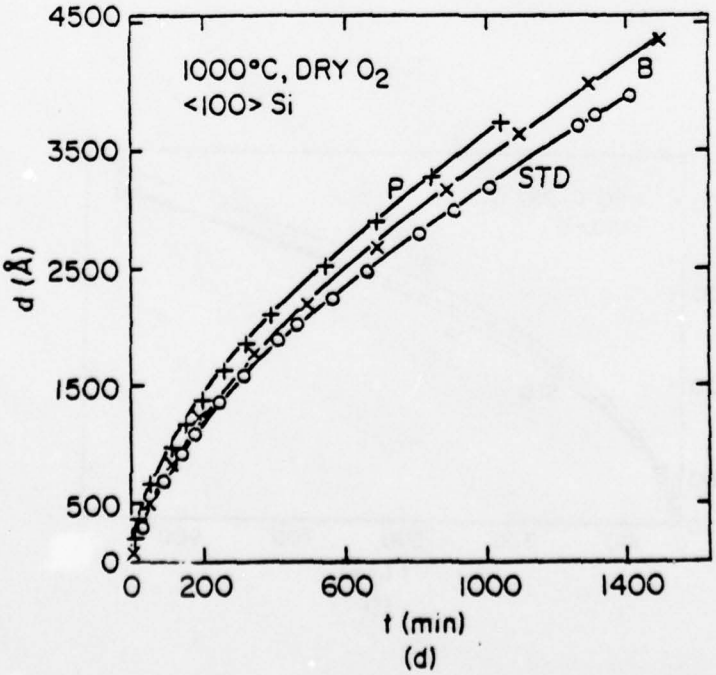
4500
3500
2500
1500
500
0
d (Å)
1000°C, DRY O2
<100> Si
B
P
STD
0
200
600
1000
1400
t (min)
(d)

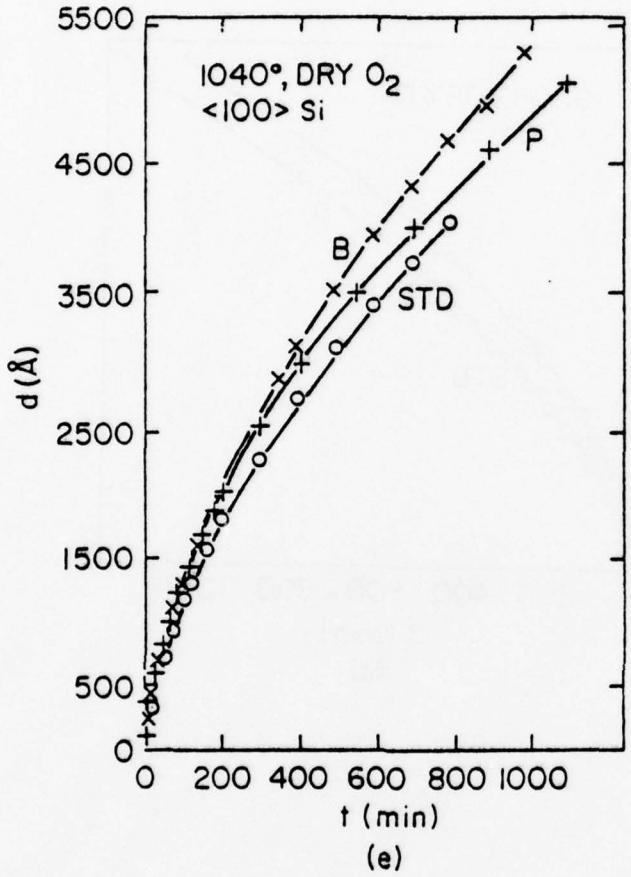
1040°, DRY O_2
<100> Si
B
P
STD
d (Å)
t (min)
5500
4500
3500
2500
1500
500
0
0 200 400 600 800 1000

(e)

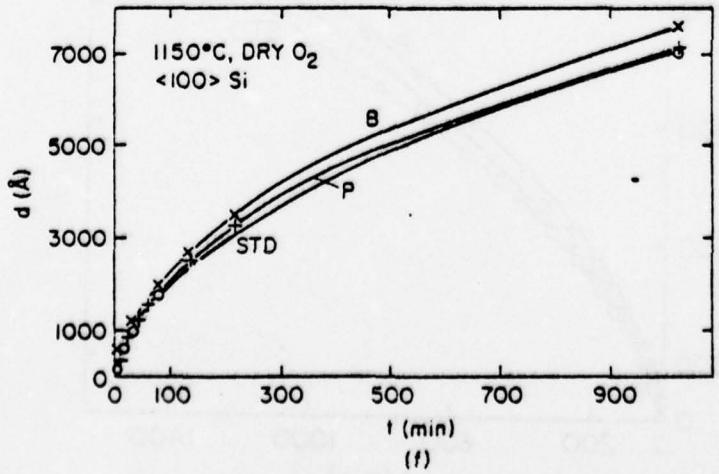
1150°C, DRY O_2
<100> Si
B
P
STD
d (Å)
t (min)
7000
5000
3000
1000
0
0 100 300 500 700 900

(f)

Figure 2 Arrhenius plots of (a) ln k_L versus 1/T and (b) ln k_P versus 1/T for the data from Table 1.

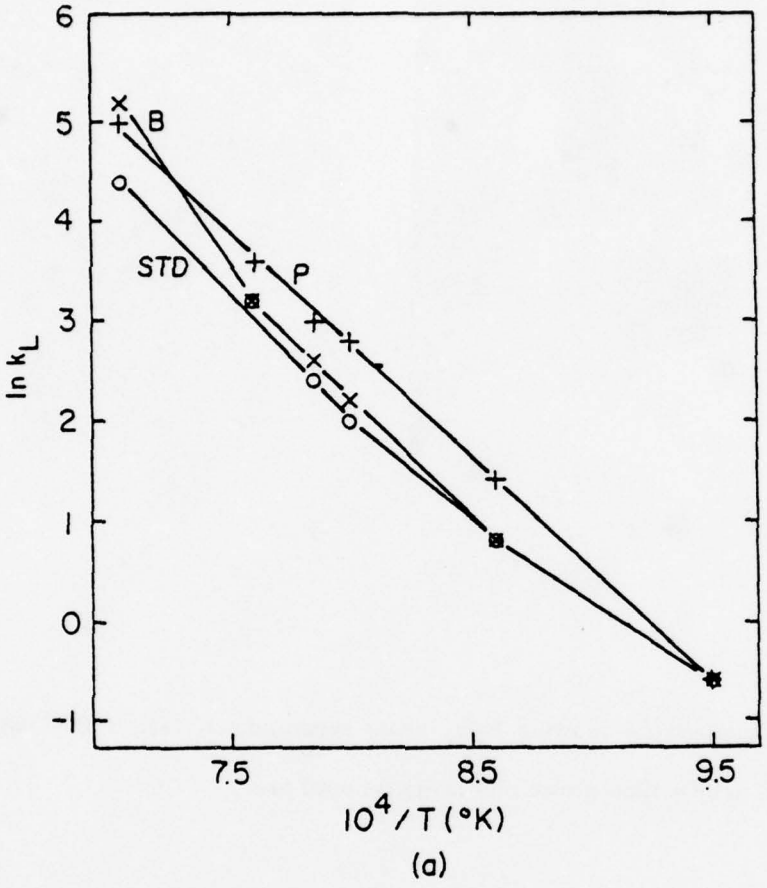

(a)

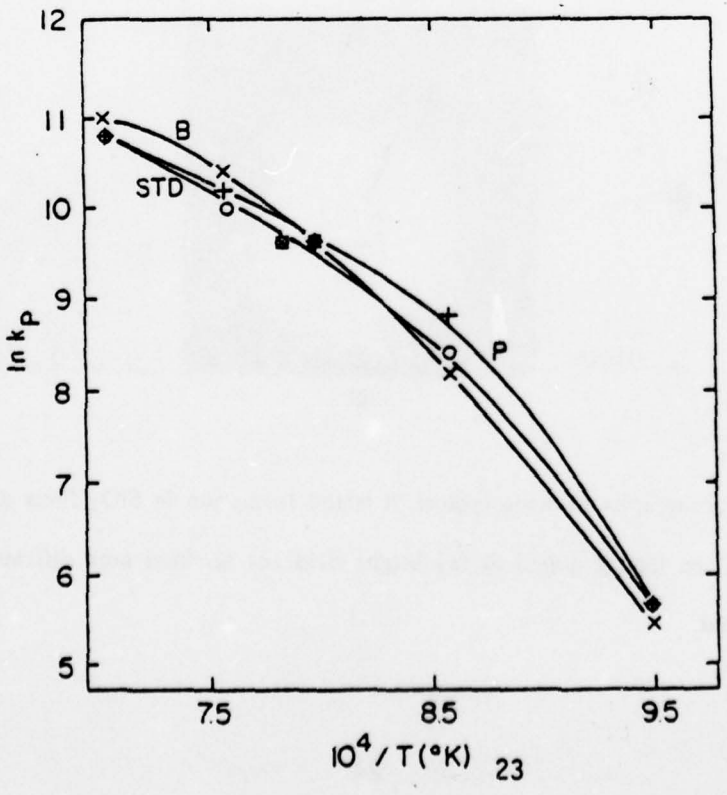

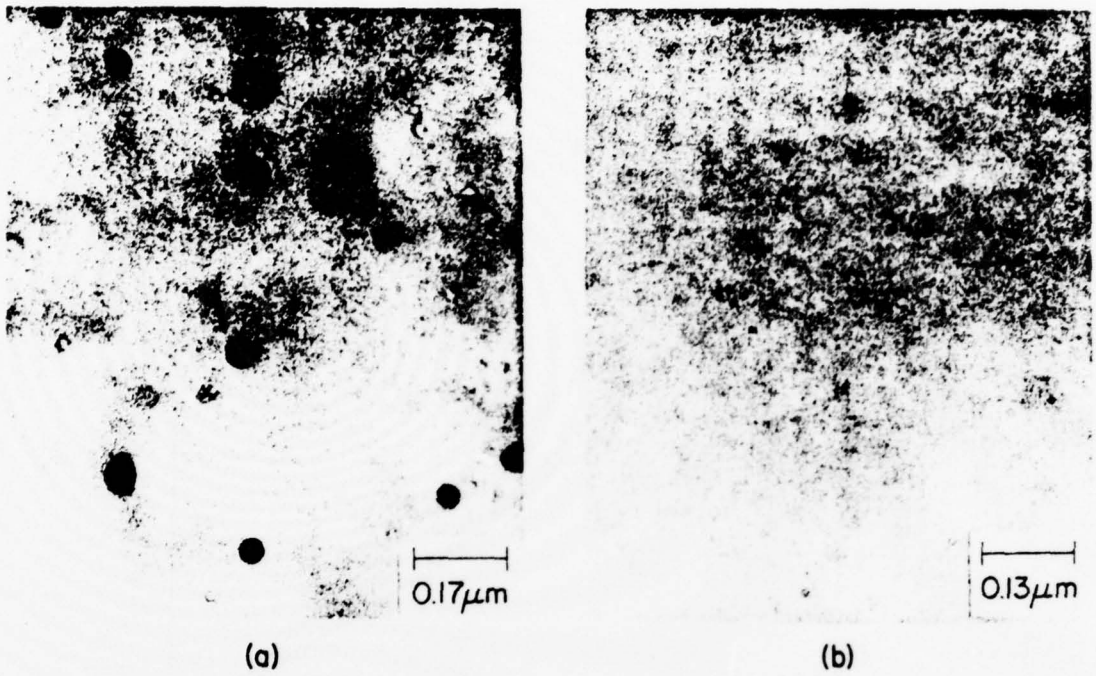

Figure 3 TEM micrographs showing B_2O_3 phase separation at (a) 1150°C and (b) 780°C in SiO_2 films grown on heavily B doped Si.

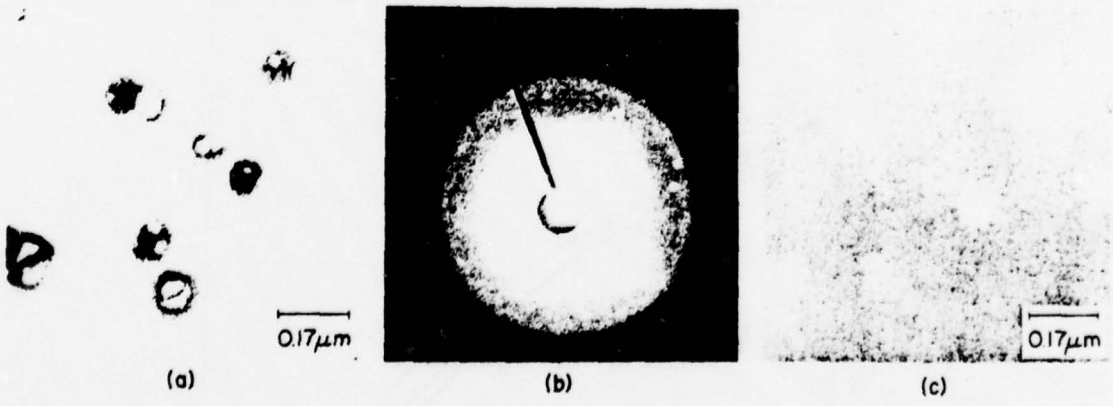

Figure 4 TEM micrographs showing typical Si island formation in SiO_2 films grown at 1150°C on lightly doped Si (a) bright field (b) selected area diffraction (c) dark field.

Table 1

Oxidation Temp.	k_L(Å/min)			k_P(Å²/min)			d_o(Å)		
°C	STD	B	P	STD	B	P	STD	B	P
780	.56	.58	.52	265	244	288	50	30	150
893	2.2	2.4	3.9	4,350	4,000	6,900	340	210	190
980	7.7	8.5	17	14,000	14,100	14,000	380	200	300
1000	12	13	21	14,300	16,000	16,000	350	350	370
1040	26	25	40	24,000	35,700	26,300	200*	200*	200*
1150	90	170	140	53,000	60,000	52,000	200*	200*	200*

- The maximum spread in k_L and k_P values is less than ± 10%
- The errors in d_o values are estimated to be ± 50 Å for STD values and ± 100 Å for B and P data. The 1150°C data has a larger error of about ± 150 Å due to having only 10 data points per curve.
- * 200 Å represents the maximum value considering a large scatter.

Table 1 Rate constants obtained from linear least squares analysis of the oxidation data.

Table 2

Temp Range	$E_{a,L}$ (eV)			$E_{a,P}$ (eV)		
	STD	B	P	STD	B	P
980°-1150°C (4 pts)	2.2	2.7	2.0	1.3	1.3	1.2
780°-1000°C (4 pts)	1.6	1.6	1.9	2.1	2.2	2.1
780°-1150°C (6 pts)	1.8	1.9	2.0	1.9	2.0	1.8
Deal and Grove (Ref 7) 900°-1200°C	2.0			1.2		
Irene and van der Meulen (Ref 13) 780°-980°C	1.5			2.3		

Table 2 **Arrhenius activation energies comparison for the high and low temperature regimes.**

References

1.) M.M. Atalla and E. Tannebaum, Bell System. Tech. J, 39, 933 (1960).

2.) F. Leuenberger, J. App. Phys., 33, 2911 (1962).

3.) A.S. Grove, O Leistiko and C.T. Sah, J. Appl. Phys., 35, 2695 (1964).

4.) B.E. Deal, A.S. Grove, E.H. Snow and C.T. Sah, J. Electrochem. Soc., 112, 308 (1965).

5.) B.E. Deal and M. Sklar, J. Electrochem. Soc., 112, 430 (1965).

6.) M. Ghezzo and D.M. Brown, J. Electrochem. Soc., 120, 146 (1973).

7.) B.E. Deal and A.S. Grove, J. Appl. Phys., 36, 3770 (1965).

8.) "Modern Aspects of the Vitreous State" Ed. J.D. Mackenzie, Butterworths and Co. Ltd., 1960, Washington. Chap. 4 on phosphate glasses by A.E.R. Westman and Chap. 5 on borate glasses by P.J. Bray and A.H. Silver.

9.) "Glass Science" Doremus, John Wiley and Sons Inc. New York, 1973 Chap. 3.

10.) R.J. Charles and F.E. Wagstaff, J. Am. Ceram. Soc., 51, 16 (1968).

11.) K.D. Kang, PhD. Thesis, Ohio State University 1962.

12.) Y.J. van der Meulen and N.C. Hien, J. Opt. Soc. Am., 64, 804 (1974).

13.) E.A. Irene and Y.J. van der Meulen, J. Electrochem. Soc., 123, 1380 (1976).

14.) E.A. Irene, J. Electrochem Soc., 121, 1613 (1974).

15.) E.A. Irene, V.J. Silvestri and G.R. Woolhouse, J. Electronic Materials, 4, 409 (1975).

16.) E.A. Irene and R. Ghez, J. Electrochem. Soc., 124, 1757 (1977).

17.) J.A. Van Vechten and C.D. Thurmond, Phys. Rev. B, 14, 3539 (1976).

LIGHT ACTIVATED STORAGE DEVICE (LASD)*

D. J. DiMaria, R. F. DeKeersmaecker, and D. R. Young
IBM Thomas J. Watson Research Center
Yorktown Heights, N. Y. 10598

Technical Assistance of J. A. Calise, F. L. Pesavento, E. D. Alley, and Silicon Process Studies Group

Typed by: Georgianna K. Grant

Abstract: A novel non-volatile semiconductor memory called the light activated storage device (LASD) is reported. It consists of a thin metal-silicon dioxide-silicon (MOS) structure with the SiO_2 layer ion implanted with impurities such as As or P which create light sensitive traps. The sites resulting from the implantation are charged ("write" operation) by using light and a moderate voltage bias to photoinject carriers from the metal or silicon contacts into the SiO_2 where some of the carriers are trapped on these sites as they traverse the oxide layer. It is discharged ("erase" operation) by using light and a low voltage bias to photoionize these trapped charges while blocking photoinjection from the contacts with the internal field of the trapped charges. The "write" and "erase" properties of this structure are investigated as a function of the ion used (As or P), ion fluence, ion energy, and oxide thickness. The LASD is shown to have reproducible cycling properties and excellent charge retention.

* This research was supported by the Defense Advanced Research Projects Agency and monitored by the Deputy for Electronic Technology, RADC, under Contract F 19628-76-C-0249.

A metal-silicon dioxide-silicon (MOS) structure is reported which is the building block for a novel type of non-volatile memory cell called the Light Activated Storage Device (LASD). The device relies upon a charge trapping region in the thermal SiO_2 layer created by implanted ions. This implanted SiO_2 layer is shown to be *charged* ("write" operation) *and discharged* ("erase" operation) with *light* at low average electric fields ($\lesssim$2 MV/cm) in the SiO_2 layer. This structure is different from those previously reported using ion implanted layers [1, 2, 3] in two respects:

(1) Because of the high temperature annealing treatment (1000°C) used after ion implantation to remove atomic displacement damage, the trapped charge centroid in a "written" device is the same as the ion distribution centroid [4]. In earlier structures, incomplete annealing [1, 2, 3] tends to favor charging near the injecting interface because of the larger numbers of traps due to atomic displacement damage effects [2]. In these structures, the centroids of the trapped charge distribution and the ion distribution are probably not the same.

(2) Previous structures do not rely on light for *charging and discharging* [1, 3]. In the MOS structures of Chen, Pickar and Sze, high electric fields are used for charging the Au implanted SiO_2 layer [1]. In the MOS structures of Jacobs and Dorda, light is used for charging Kr or N implanted SiO_2 layers while thermal energy (samples are heated to 500°C) is used for discharging [3].

The LASD also avoids problems encountered with devices which use charge trapping layers formed by other means besides ion implantation. One example is the metal-silicon nitride-silicon dioxide-silicon (MNOS) structure which requires high electric fields for "write" and "erase" operations [5]. Degradation of the MNOS structures with cycling is believed to be caused by the high fields at the Si-SiO_2 interface. LASD structures have another advantage over MNOS structures since the charge trapping layer can be placed at any position in the oxide layer. In MNOS structures, the entire nitride layer contains traps for both electrons and holes [7] which inherently can cause charge redistribtuion effects. Another example is the

floating gate avalanche injection type MOS (FAMOS) structure which relies on a floating polycrystalline Si gate electrode embeded in the SiO_2 layer [6]. These structures are more susceptible to charge leakage at any weak spots in the oxide layer from this polycrystalline Si layer due to its continuous nature as opposed to the discrete trapping sites of the LASD.

The LASD structures are easy to fabricate. The MOS samples used in this study were formed by oxidizing 0.1 Ω-cm p-type <100> Si in dry O_2 at 1000°C to SiO_2 thicknesses of approximately 500 Å and 1400 Å. As and P ions were then implanted into the SiO_2 layer at the energies and fluences given in Table I. The centroids for electrons trapped on sites related to the implanted ions as deduced from photo I-V measurements (which have the same values as the centroids for the ions [4]) are also given in this table. After implantation, the oxide surfaces were cleaned of hydrocarbons and metals using a treatment described by Irene [8] only without HF. Then a 1000°C anneal for 30 minutes in N_2 was done to remove positive charges and traps created by ionization effects and traps caused by atomic displacement damage. Finally thin Al electrodes (130 Å) were deposited (circular area of 5.2×10^{-3} cm^2) followed by a 400° C forming gas anneal for 20 minutes. All oxide thicknesses in Table I were measured using ellipsometry.

The apparatus used to determine the charge state of the LASD structures were 1 MHz capacitance-voltage (C-V) and photocurrent-voltage (photo I-V) set-ups which have been described previously [7]. Capacitance-voltage curves as in Fig. 1 give a measure of the trapped charge-centroid product, while the photo I-V measurements give the centroid and the trapped charge independently. Charging and discharging were accomplished with 900 W xenon and 60 W deuterium lamps capable of giving photon fluxes in the range from 10^{12} to 10^{16} photons/(cm^2-sec) at the energy or energies of interest here. Filters or a monochromator were used to give the desired light energy or energies. Direct contact to the semitransparent Al dots was made with a polished tungsten probe 5 mils in diameter positioned near the edge

of the dot. Probe shadowing of the light active gate region was experimentally shown to be negligible for this small probe diameter.

Sites related to various ions implanted into the SiO_2 layer of an MOS structure such as P and As can be charged or discharged using light under the procedure to be described next. Light within the proper energy range can photoinject electrons from the Si or Al contacts into the SiO_2 layer for positive and negative gate bias, respectively. Some of these electrons will be trapped in the ion implanted region of the oxide with a capture probability proportional to the product of the number of empty traps per unit area and the capture cross section for the sites related to the implanted ions [9,10]. However, simultaneously the same light energy used to inject the electrons from the contacts can discharge the traps if the trapped electron photoionization energy is comparable to or less than the energy required for injection. This process is shown in Fig. 2. For a given applied voltage bias, the traps will fill to some steady state level determined by the ratio of the time constants of capture and photoionization processes [9]. This is the "write" operation of the LASD structure. The time dependence of the volume density of trapped electrons n_t is

$$\frac{dn_t}{dt} = \frac{N_t - n_t}{\tau_c} - \frac{n_t}{\tau_p} \tag{1}$$

with

$$\tau_c = \frac{q}{J\sigma_c} \tag{2}$$

and

$$\tau_p = \frac{1}{F_p \sigma_p} \tag{3}$$

where N_t is the volume density of traps, τ_c is the capture time constant, τ_p is the photoionization time constant, q is the electron charge, J is the injected current per unit area [9, 10], F_p is the photon flux, σ_c is the capture cross section, and σ_p is the photoionization cross section. Steady state is reached when $dn_t/dt=0$, and from Eq. 1 this condition gives the steady state trapped electron density $n_{t_{ss}}$ by

$$n_{t_{ss}} = \frac{N_t}{1 + \frac{\tau_c}{\tau_p}} \quad . \tag{4}$$

Increasing the number of traps associated with the implanted ions or the magnitude of the capture cross section relative to the photoionization cross section will decrease the time required to "write" the LASD structure to a given charge state (see Eq. 1) and allows a larger steady state density of trapped charge to be obtained (see Eq. 4). In addition to changing the magnitudes of N_t, σ_p, and/or σ_c, faster charging and a larger value of $n_{t_{ss}}$ can be obtained by increasing J with a larger gate voltage bias thereby allowing more "hot" electrons to surmount the Schottky lowered barrier at the photoinjecting interface [11]. This internal photoemission current also could be enhanced by increasing the photon flux ($J\alpha F_p$ [9]) which would increase the charging rate (see Eq. 1). However, since $\tau_p^{-1} \alpha F_p$, the steady state charge density would not be affected.

To "erase" the LASD structure once it is charged, electron capture has to be suppressed and photodetrapping of the trapped electrons enhanced. This can be done by preventing electron injection from the contacts by reducing either the light energy or the applied voltage for a given light energy as shown in Figs. 2b and 2c, respectively. Photodetrapping is described by Eq. 1 with the omission of the capture process (first term on the right hand side of the equation) if retrapping is negligible. The process shown in Fig. 2b would only apply for trapped electron photoionization energies less than those required for carrier injection from the contacts [9, 12]. In Fig. 2c where the photoionization energy of the trapped electrons is comparable to or greater than that required for carrier injection, the built-in field of the negative trapped space charge is used to block photoinjection from the contacts at a low applied gate voltage bias but permit photodetrapping [13].

In Fig. 1, capacitance-voltage curves are shown for an MOS structure implanted with 1 x 10^{14} As^+/cm^2 which is used as an LASD device. The flat-band voltage shift ΔV_{FB} between the

various curves with respect to curve A indicates their charge state, since

$$\Delta V_{FB} = \frac{\bar{x}q}{\varepsilon} \int n_t \, dx \qquad (5)$$

where $\bar{x}$ is the centroid of the trapped negative charge measured from the metal-SiO_2 interface, L is the oxide thickness, and ε the low frequency dielectric constant of SiO_2 [14]. Curve A corresponds to the uncharged virgin structure. Curve B corresponds to the charged structure where the electron traps in the implanted region have been filled in 15 sec. to a steady state value dependent on the light energy and voltage bias indicated. This is the "written" state. Curve C corresponds to the discharged structure after photoionization for 47 min. at the light energy and voltage bias indicated. This is the "erased" state.

The capture cross sections, photoionization cross sections, centroids for the negative trapped charge, and the total number of traps have been determined for sites related to the implanted As and P in the oxide layer of the MOS structures used here. The details of these measurements will be reported in future publications, however some of the measured values will be used here so that comparisons can be made with theoretical predictions. The photoionization cross section σ_p is essentially identical for both ions with values ranging from 10^{-18} to 10^{-17} cm^2 for light energies from 3.5 to 5.5 eV. Note that light energies greater than 4 eV and 3.2 eV are needed for photoinjection from Si and Al contacts, respectively [11]. The capture cross sections for the dominant trapping sites are significantly different with implanted As having a value of $\approx 1 \times 10^{-15}$ cm^2 compared to a value of $\approx 1 \times 10^{-17}$ cm^2 for P. Hence, As implanted LASD structures are inherently easier to "write". This was verified experimentally by comparing the trapping characteristics (similar to Fig. 1) of As and P samples which had identical numbers of traps and identical centroid positions (samples AS3 and P2, AS5 and P1). Some detailed differences between samples with different implantation energies due to optical interference effects [7] were seen. The standing wave pattern of the light intensity in the oxide film overlapped the trap distribution differently especially in the 1300 - 1400 Å thick

films depending on the implantation energy [7]. More charging was seen under identical conditions on samples where minima in the interference pattern overlapped a significant portion of the trap distribution thereby decreasing photodetrapping. For example, P2 (40 keV P) charged to a larger steady state value of trapped charge taking the centroid difference into account than P1 (30 keV P). The centroid of this trapped charge in P2 (measured using the photo I-V technique) was near the appropriate minimum in the standing wave pattern.

The steady state value of the trapped charge $n_{t_{ss}}$ under constant J was observed to be proportional (to within 30%) to the ion fluence and therefore the trap density on samples AS2, AS3, and AS4. Samples with large fluences (for example, comparing AS4 to AS3) were "written" to the same charge state faster under equivalent charging conditions because of the larger number of traps. Calculated values of the total steady state trapped charge were smaller than the measured values by 50%. The calculated values were obtained by integrating $n_{t_{ss}}(1+\tau_c/\tau_p)=N_t$ over the oxide thickness taking into account the spatial variation of F_p [7] and $n_{t_{ss}}$ where it was assumed that the trapped charge had the same spatial variation as the implanted ions [4].

Once "written" the LASD structures were "erased" in the manner shown in Fig. 2c as previously described due to the energy depth from the SiO_2 conduction band of traps related to either implanted P or As. These deep traps have an optical threshold of $\approx$ 4 eV and will be discussed in detail in future publications. The rate at which the LASD structures could be photodetrapped ("erased") from the same charge state was shown experimentally to be independent of ion fluence, implantation energy (taking into account the differences in the ion distributions and how they overlap the standing wave pattern of the light intensity in the oxide films), and the ions used (As and P have the same photoionization cross section - photon energy dependence).

Compensating effects such as positive charge build-up at the Si-SiO_2 interface were ruled out as an explanation of the shift of the C-V curve to position C from position B in Fig. 1 by

using the photo I-V technique [13] which can separate bulk charging or discharging effects from Si-SiO_2 interface effects to which the data of Fig. 1 are sensitive [14]. Using the photo I-V technique at various stages of the photodetrapping ("erase") process to track both the centroid and trapped charge, it was clearly shown that *negative* trapped charge was being *removed* from the bulk of the SiO_2 film. The photo I-V technique was also used to show that the centroid of the trapped charge distribution and the implanted ion distribution are identical [4] and these measurements will be discussed in future publications.

As seen in Fig. 1, curve C indicated $\approx$ 1V of negative charge (compared to the virgin curve A) still in the oxide after the photodetrapping ("erase") step. Small changes in the gate bias from V_g=0 to V_g=–0.9 V to maintain a very small total oxide voltage drop (see Fig. 2c) had little effect in the removal of this charge. The LASD could be switched very reproducibly between curves C and B in Fig. 1 during subsequent "write"-"erase" cycles. This 1V of charge is again due to a minimum in the intensity pattern created in the oxide film by optical interference [7]. This was demonstrated experimentally by comparing the photodetrapping ("erase") characteristic of LASD structure AS1 (490 Å of SiO_2, 20 keV As) with AS3 (1415 Å of SiO_2, 80 keV As) and AS5 (1433 Å of SiO_2, 60 keV As). AS1 has no minima in the intensity pattern overlapping the trap distribution which allowed it to be completely discharged back to its virgin state A. The centroid for the 1V of remaining charge in AS5 was found to be near the appropriate minimum in the intensity pattern.

All LASD structures in Table I showed excellent charge retention characteristics in the dark as demonstrated in Fig. 3 for a grounded gate and substrate condition. Even when a gate voltage bias of $\approx$ + 40 V was applied less than 18% of the total trapped charge was removed under dark conditions.

The most convenient and practical way to operate the LASD is using a light source of some fixed energy or fixed energy range and then changing the voltage bias to "write" or "erase" it. As demonstrated here, increasing the number of traps by using larger ion fluences

or increasing the capture cross section to photoionization cross section ratio will increase the speed of the "write" operation to a given charge state. The "erase" operation can be accelerated by using implanted ions which create shallower traps and therefore give larger photoionization cross sections at least at lower photon energies. These shallower traps must still permit charging ("write" operation) and show good charge retention. The LASD structures can also be "written" with avalanche injection of electrons from the Si substrate or by high field Fowler-Nordheim tunneling of electrons from the Si or Al electrodes and then "erased" using photodetrapping. However, in this mode the advantages of using low applied voltages for "writing" the LASD structures with light would be lost.

ACKNOWLEDGEMENTS

The authors would like to acknowledge the critical reading of the manuscript by M. I. Nathan; the sample preparation by the Silicon Process Studies Group; the thin Al metallization by E. D. Alley; and the experimental assistance of J. A. Calise and F. L. Pesavento.

REFERENCES

1. L. I. Chen, K. A. Pickar, and S. M. Sze, Solid St. Electron *15* 979 (1972).
2. N. M. Johnson, W. C. Johnson, and M. A. Lampert, J. Appl. Phys. *46*, 1216 (1975).
3. E. P. Jacobs and G. Dorda, Solid St. Electron. *20*, 367 (1977).
4. D. J. DiMaria, D. R. Young, R. F. DeKeersmaecker, W. R. Hunter, and C. M. Serrano, The Electrochemical Society Fall Meeting, Atlanta, Georgia, 1977, Abstract No. 212 (unpublished).
5. D. Frohman-Bentchkowsky and M. Lenzlinger, J. Appl. Phys. *40*, 3307 (1969).
6. D. Frohman-Bentchkowsky, ISSCC Dig. of Tech. Papers *15*, 80 (1971).
7. D. J. DiMaria and P. C. Arnett, IBM J. Res. Devel. *21*, 227 (1977), and references contained therein.
8. E. A. Irene, J. Electrochem. Soc. *121*, 1613 (1974).
9. D. J. DiMaria, F. J. Feigl, and S. R. Butler, Phys. Rev. B *11*, 5023 (1975).
10. D. J. DiMaria, J. M. Aitken, and D. R. Young, J. Appl. Phys. *47*, 2740 (1976).
11. B. E. Deal, E. H. Snow, and C. A. Mead, J. Phys. Chem. Solids *27*, 1873 (1966).
12. D. J. DiMaria and F. J. Feigl, Phys. Rev. B *9*, 1874 (1974).
13. D. J. DiMaria, J. Appl. Phys. *47*, 4073 (1976).
14. A. S. Grove, *Physics and Technology of Semiconductor Devices* (Wiley, New York, 1967), Chap. 9.

TABLE I

DESCRIPTION OF SAMPLES USED IN THIS STUDY

SAMPLE NUMBER	OXIDE THICKNESS Å	ION TYPE	FLUENCE ions/cm^2	ENERGY keV	CENTROID Å
AS1	490	As	1×10^{13}	20	190
AS2	1423	As	3×10^{12}	80	535
AS3	1415	As	1×10^{13}	80	570
AS4	1405	As	1×10^{14}	80	525
AS5	1433	As	1×10^{13}	60	470
P1	1283	P	1×10^{13}	30	420
P2	1277	P	1×10^{13}	40	545

FIGURE CAPTIONS

Fig.1 High frequency (1 MHz) capacitance as a function of applied gate voltage on LASD structure AS4 where curves A, B, and C correspond to:

A - The virgin sample AS4 after fabrication.

B - AS4 after charging traps for 15 sec. to a steady state condition with V_g = -29 V and the light from a deuterium lamp with a 5.5 eV low frequency pass filter (to prevent possible hole injection from the contacts and trapping). The current measured in the external circuit during this 15 sec. time interval decayed from 5.3 x 10^{-9} A to 3.2 x 10^{-9} A. This corresponds to the "write" operation.

C - AS4 after photodetrapping of trapped charge for 47 min. from charging step B. V_g=0 V and the same light energies as in step B were used. This corresponds to the "erase" operation.

Fig.2 (a) Energy band diagram of MOS LASD structure showing electron injection from the metal (Al) into the SiO_2 conduction band by internal photoemission at a light energy $\hbar\omega_1$ under a negative gate voltage bias, subsequent transport and trapping of some of the injected electrons in the ion implanted region of the SiO_2 structure, and finally photoionization of some of the trapped electrons by the light which penetrates through the semitransparent metal gate electrode. Dashed arrows indicate movement of electrons.

(b) Trap photoionization at a light energy $\hbar\omega_2$ which is less than the energy barrier height at the Al-oxide interface $\phi_{B_{Al}}$ for photoinjection from the metal. The trapped electron energy depth from the oxide conduction band E_t has to be less than $\phi_{B_{Al}}$ if internal photoemission from the metal contact is to be suppressed under a negative gate bias condition as shown.

(c) Trapped electron photoionization for cases where $E_t > \phi_{B_{Al}}$. For this case, a gate voltage bias of -0.9 V is applied to cancel the effect of the contact

potential difference between the Al gate and p-Si substrate [14] (total voltage drop across the oxide is 0 V). Photoionization of trapped negative charge is favored by the built-in field due to this charge (as shown by the upward bending of the oxide bands). Electron injection from the contacts by internal photoemission is suppressed because the injected electrons can not flow against the built-in fields of the trapped charge.

Fig.3 Flat-band voltage shift ΔV_{FB} as a function of time under dark stressing conditions of V_g=0 V on sample AS5 which was initially charged to 8.25 V.

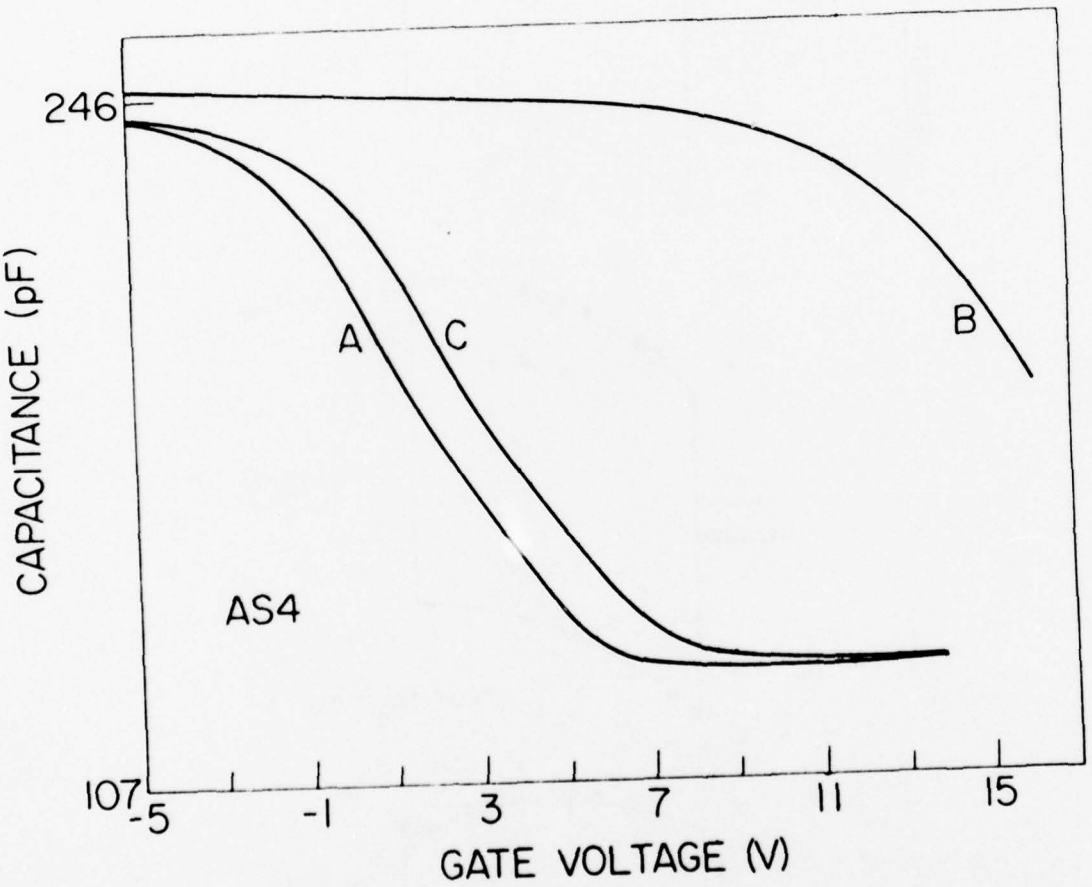

Figure 1.

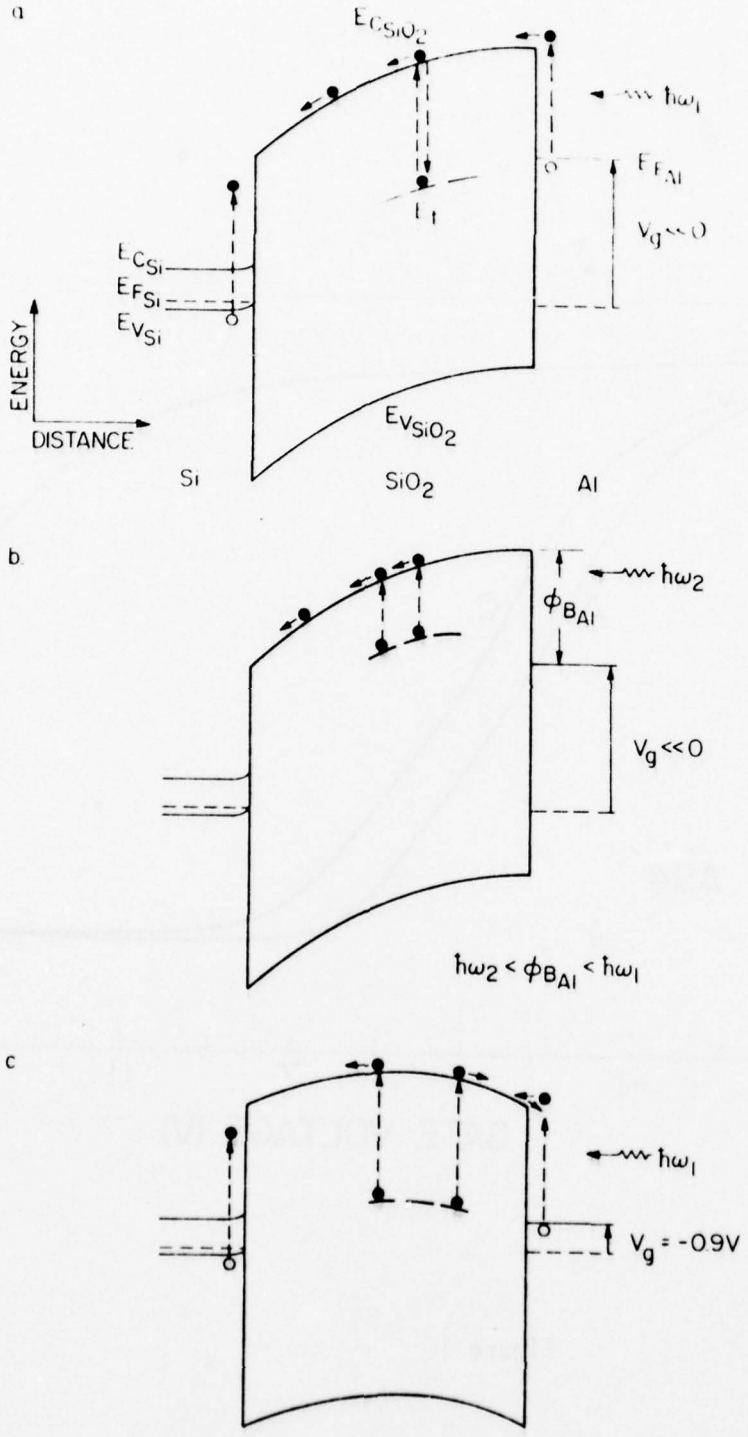
a
$E_{C_{SiO_2}}$
$\hbar\omega_1$
$E_{F_{Al}}$
E_t
$V_g \ll 0$
$E_{C_{Si}}$
$E_{F_{Si}}$
$E_{V_{Si}}$
ENERGY
DISTANCE
$E_{V_{SiO_2}}$
Si
SiO_2
Al
b
$\hbar\omega_2$
$\phi_{B_{Al}}$
$V_g \ll 0$
$\hbar\omega_2 < \phi_{B_{Al}} < \hbar\omega_1$
c
$\hbar\omega_1$
$V_g = -0.9V$

Figure 2

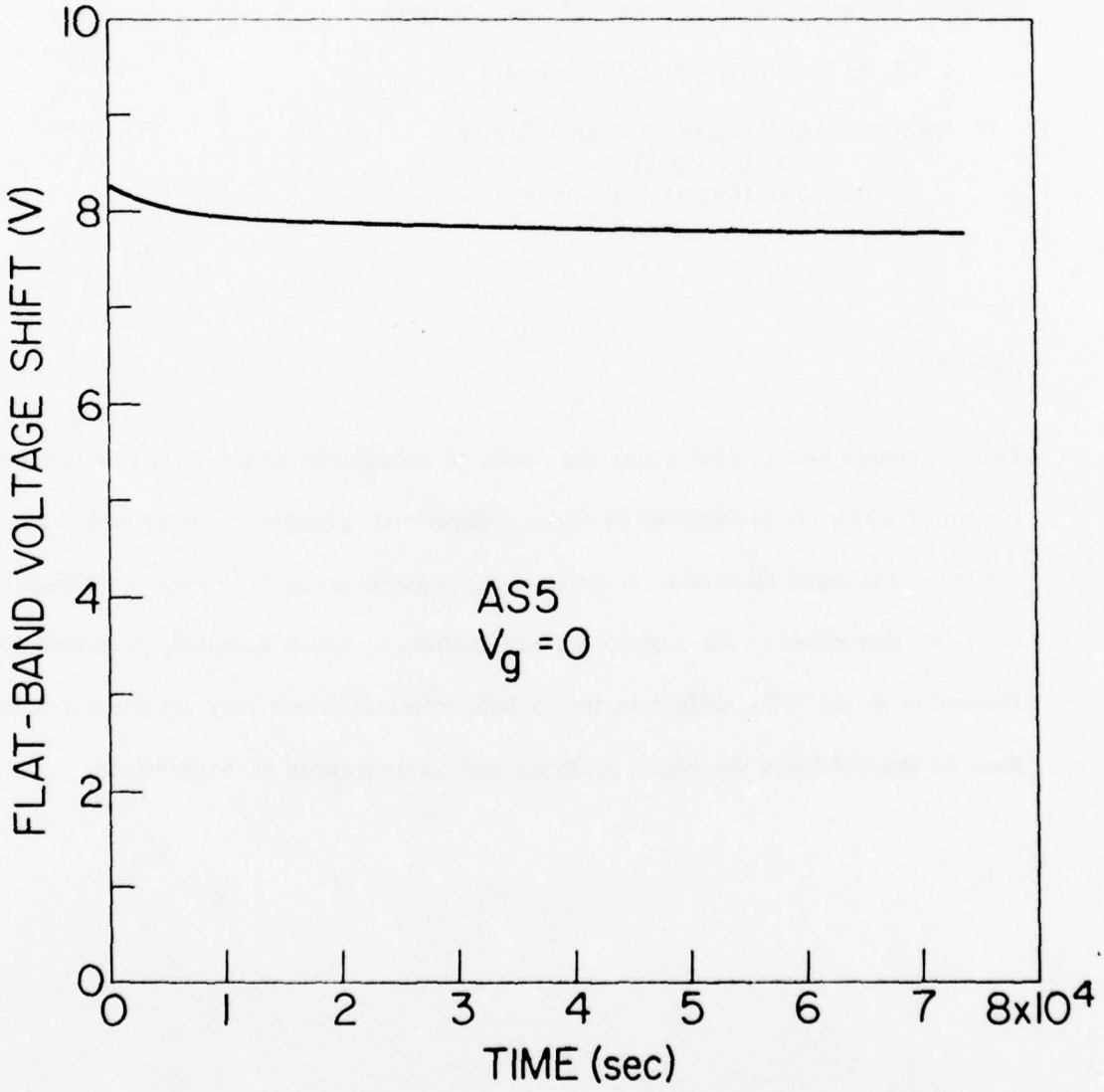
FLAT-BAND VOLTAGE SHIFT (V)
10
8
6
4
2
0
AS5
$V_g = 0$
0
1
2
3
4
5
6
7
8x10⁴
TIME (sec)

Figure 3

Exciton Creation and Transport in SiO_2 as a Cause of Surface State Generation in MOS Structures

Z. A. Weinberg and G. W. Rubloff

IBM Thomas J. Watson Research Center
P. O. Box 218
Yorktown Heights, NY 10598

ABSTRACT

Positive charge and surface states are found to accumulate at the Si-SiO_2 interface in MOS structures which are illuminated by vacuum ultraviolet photons (>9 eV) with a negative bias applied to the metal electrode. A series of experiments seems to rule out the obvious explanations for this effect. We suggest an explanation in which excitons, generated by photon absorption in the SiO_2, diffuse to the Si-SiO_2 interface where they are separated into a free electron absorbed into the silicon substrate and a hole trapped at the interface.

It is well known that the Si-SiO_2 interface in MOS (metal-oxide-silicon) structures exhibits a strong trapping capability for holes created in its vicinity or transported across it.[1-6] It was recently observed[1] that positive charge accumulates at the Si-SiO_2 interface under conditions where free holes are not thought to arrive at this interface, namely, when the structure is illuminated with vacuum ultraviolet (VUV) photons (which are strongly absorbed in SiO_2) and the applied negative bias prevents holes from reaching the Si-SiO_2 interface. The purpose of this letter is to describe several experiments aimed at investigating the source of this phenomenon and to suggest that holes may be carried through the SiO_2 film by diffusion of excitons.

The MOS devices consisted of thermally grown SiO_2 films on p-type, 2 Ωcm, (100) silicon substrates. The oxides of Figs. 1 through 3 were grown in a dry O_2 atmosphere at 1000°C with a post-oxidation anneal of 5 min. in N_2 at 1000°C and a post-metallization anneal of 20 min. in forming gas (F. G. : N_2/H_2 mixture) at 400°C. The oxides of Fig. 4 were grown by a dry-wet-dry process with a similar post-oxidation anneal as above but with the F. G. anneal done prior to metallization. The aluminum electrodes were prepared by a double metallization procedure: first a thin array of semitransparent dots (100-200 Å thick, 1.25 mm diameter) was evaporated (from an RF heated source) and then overlayed with a thicker array of dots (2000 Å thick, 0.25 mm diameter) to provide a pad for bonding. The device was bonded on a header and mounted in a holder that contained a metallic shield with an aperture (1 mm in diameter) overlapping the aluminum electrode. This shield had a double purpose: it prevented exposure of the unmetallized oxide and it collected secondary electrons emitted from the electrode. It was biased positively (15 v) with respect to the electrode. This precaution ensured the proper reading of the current through the oxide, which was measured on the substrate side of the device. The holder could be rotated out of the incident light beam to allow the measurement of the incident photon flux by detecting the fluorescence of a sodium salicylate layer.[7] VUV light was obtained from a H_2 discharge and dispersed by a McPherson

model 225 monochromator using an Al/MgF_2 coated grating of 1200 l/mm.

The total amount of positive charge accumulated at the $Si\text{-}SiO_2$ interface after a period of illumination was measured by the negative shift in the standard high-frequency (1 MHz) C-V (capacitance-voltage) curve. It was previously established that the charge resides at or very near the $Si\text{-}SiO_2$ interface.[1] It is well known that the density of hole traps and their conventional separation into fixed oxide charge and surface states are strongly process dependent[4,5]; accordingly, we have observed large variations between different batches (or runs). As a result, the data presented below will be discussed only qualitatively.

The effect of the accumulation of positive charge at the $Si\text{-}SiO_2$ interface under illumination at 10.2 eV is illustrated in Fig. 1, which is a plot of the negative shifts in C-V curves as a function of illumination time. The linear dependence exhibited in the figure was found to be typical, an important feature that allows us to measure successive incremental shifts on the same device as a function of experimental variables. Such data are given in Figs. 2 and 3 showing the dependence of the effect on photon energy and applied bias, respectively. Fig. 4 shows a comparison of the effect for devices with various oxide thicknesses.

There are several processes which may explain the observed effects. It should be noted that hole or positive ion diffusion to the $Si\text{-}SiO_2$ interface is prevented by the applied bias and that negative ion drift is unlikely to result in positive charge at that interface. The explanations that must be considered are:

1. Photon processes:
   (a) Penetration of the illuminating light to the $Si\text{-}SiO_2$ interface.
   (b) Penetration of lower energy photons produced by the recombination of hole-electron pairs (photoluminescence).

2. Electronic processes:

(a) Impact ionization of traps at the Si-SiO_2 interface by hot electrons.

(b) Exciton diffusion to the Si-SiO_2 interface.

3. Lattice processes:

(a) Propagation of phonon packets (solitons) produced by the energy given off in non-radiative hole-electron recombination.

(b) Others, such as oxide shrinkage due to relieved strains, as proposed by Ma[8], propagation of dislocations, etc.

To assess the possibility of photon penetration to the Si-SiO_2 interface (item 1a) one needs to know the absorption length of these photons in SiO_2. Two sources are available for this information: Philipp's reflectance experiments on fused and crystalline quartz[9] and Powell's transmission experiments[10] on thermally grown oxide windows (580 Å) produced by etching-off an aperture in the silicon substrate. Both sources give values for the absorption length of about 410, 180, and 100 Å at 9.7, 10.0, and 10.2 eV respectively. Assuming that these values also apply to our oxides, an additional thickness of 1000 Å of SiO_2 will attenuate the light transmitted through it at 10.2 eV by a factor of about 10^4. Such strong attenuation is completely inconsistent with the much smaller thickness dependence of the effect shown in Fig. 4.

The photoluminescence explanation (item 1b) is unlikely since low energy photons (<9 eV) do not produce effects similar to those observed here.[11] Furthermore, an appreciable photoluminescence efficiency (>10%) near 9-10 eV would be required to explain the data of Fig. 2, but this is ruled out by results of previous experiments with a shallow diode buried under the oxide.[12]

Two facts argue against the hot electron explanation (item 2a). First, as shown in fig. 3, the effect decreases when the magnitude of the applied negative bias is increased. Second, the effect was not observed in experiments where hot electrons were photoinjected into the oxide from the aluminum by photons of energy below 9 eV and in which a similar magnitude of total charge was transported across the oxide.

There exists the possibility that traveling, strongly localized phonon packets with solitonic properties (item 3a) could propagate across long distances without much attenuation.[13] Conceivably such solitons could be created from the energy released in hole-electron recombination processes (~9 eV). However, we believe that this alternative is less likely than the exciton explanation. Other lattice propagation phenomena, including sample heating, would appear to be ruled out by the relatively low illumination intensity of about 10^{12} photons/cm^2-sec.

Excitons (item 2b) are believed to be an important feature of the optical spectra of SiO_2. Both experimental and theoretical studies suggest that the first strong absorption peak in SiO_2 is due to excitons.[14,15] Electron-hole interactions may be significant at higher photon energies as well.[15] It is therefore reasonable to hypothesize that excitons could produce the effects we have observed. We shall now discuss some aspects of the data of Figs. 2-4 in light of this hypothesis.

A comparison of the spectral dependence of the effect (Fig. 2) with the optical absorption spectrum of SiO_2 indicates that factors other than the photogeneration rate of excitons affect the spectral dependence. In particular, excitons created closer to the Al-SiO_2 interface may recombine, dissociate, or be absorbed into the Al more rapidly than excitons created further from the Al. Thus a complicated spectral dependence might arise, determined by the spatial distribution of exciton annhiliation as well as production.

The field dependence shown in Fig. 3 could be caused by field ionization of the excitons, which increases at higher fields, although the field dependence of hole trapping and of electron-hole annhiliation at the Si-SiO_2 interface are further complications. The thickness dependence shown in Fig. 4 would require a diffusion length for the excitons of order 500 Å. Whether the transport and decay mechanisms of excitons in SiO_2 would permit such a substantial diffusion length remains to be determined.

In summary, the observation of positive charge accumulation at the Si-SiO_2 interface under VUV photon illumination and negative gate bias is surprising. We suggest that diffusion of photogenerated excitons from the absorbing region near the Al-SiO_2 interface to the Si-SiO_2 interface may be the source of the observed phenomena. More work is needed, however, to determine with certainty whether exciton transport in SiO_2 accounts for the observed effects and, if so, what is the nature of exciton dynamics and decay mechanisms in SiO_2. The findings presented here may add an important insight to the understanding of the processes occuring in SiO_2 under high energy photon or particle bombartment.

ACKNOWLEDGEMENTS

The authors are grateful to H. R. Philipp for supplying a detailed table of the optical constants of fused quartz and to P. M. Solomon for bringing to our attention Powell's report. The authors appreciate the illuminating discussions with D. J. DiMaria, S. T. Pantelides, A. B. Fowler, and D. R. Young. The technical assistance of A. Marx, J. Donelon, E. Alley, J. Kuran, and the Si facility at IBM is kindly acknowledged.

REFERENCES

1. D. J. DiMaria, Z. A. Weinberg, and J. M. Aitken, J. Appl. Phys. 48, 898 (1977).

2. R. J. Powell, J. Appl. Phys. 46, 4557 (1975).

3. P. S. Winokeur and M. M. Sokoloski, Appl. Phys. Lett. 28, 627 (1976).

4. J. M. Aitken and D. R. Young, to be published in IEEE Trans. Nucl. Sci. NS-24, (Dec. 1977).

5. K. G. Aubuchon, IEEE Trans. Nucl. Sci. NS-18, 117 (1971).

6. J. R. Srour, S. Othmer, O. L. Curtis Jr., and K. Y. Chiu, IEEE Nucl. Sci. NS-23, 1513 (1976).

7. J. A. R. Samson, Techniques of Vacuum Ultraviolet Spectroscopy (Wiley, New York 1967).

8. T. P. Ma, Appl. Phys. Lett. 27, 615 (1975).

9. A detailed table of optical constants of fused quartz was supplied by H. R. Philipp. See also H. R. Philipp, J. Chem. Phys. Solids, 32, 1935 (1971).

10. R. J. Powell, Government Report No. AFGL-TR-0017 (1976).

11. We did observe C-V shifts with photons below 9 eV, but these shifts occur with much lower efficiency than those shown in Fig. 2 for equal illumination intensities and display a strong field dependence opposite to that of Fig. 3.

12. Z. A. Weinberg, Appl. Phys. Lett., 17, 437 (1975).

13. A. C. Scott, F. Y. F. Chu, and D. W. McLaughlin, Proceedings of the IEEE, 61, 1443 (1973).

14. J. R. Chelikowsky and M. Schluter, Phys. Rev. B15, 4020 (1977) and references therein.

15. S. T. Pantelides, to be published in Comments on Solid-State Physics.

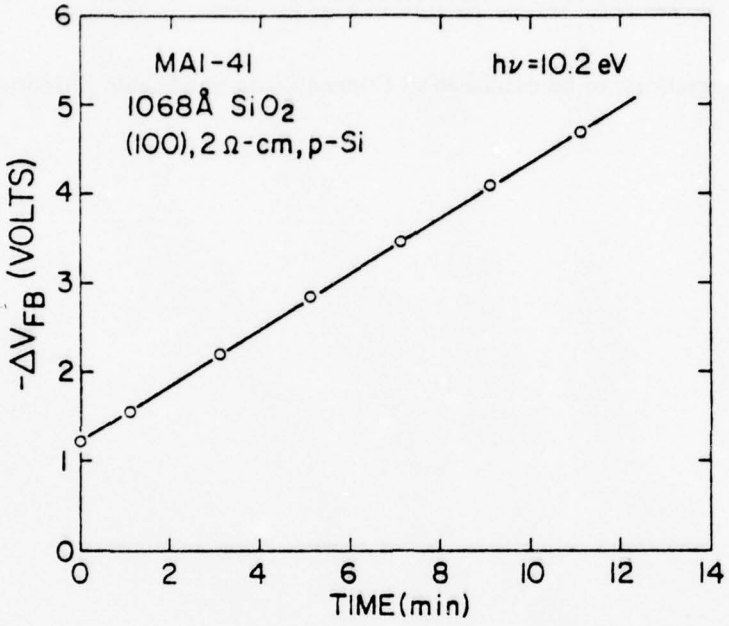

Fig. 1 Typical negative flat-band voltage shifts as a function of the accumulated time of illumination with 10.2 eV photons. The voltage applied to the gate of the MOS capacitor was −11 V. The current through the oxide was 1.4×10^{-9} amp.

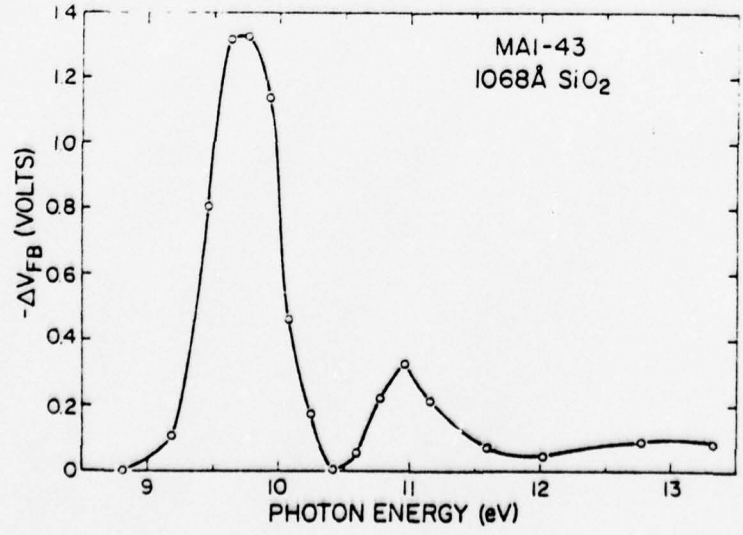

Fig. 2 Successive incremental flat-band voltage shifts as a function of photon energy. The voltage applied to the gate of the MOS capacitor was −11 V. The data were corrected for the variations in the photon flux incident on the sample but not for reflection, which can vary by up to 20%.

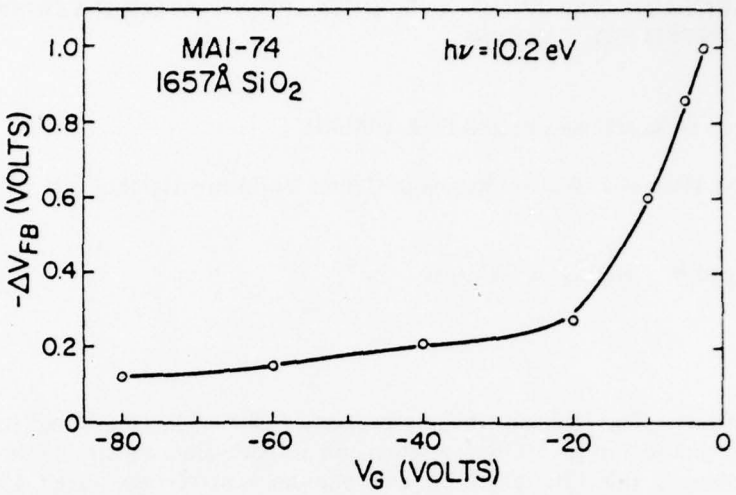

Fig. 3 Successive incremental flat-band voltage shifts as a function of the applied voltage to the aluminum electrode. The photon energy was 10.2 eV.

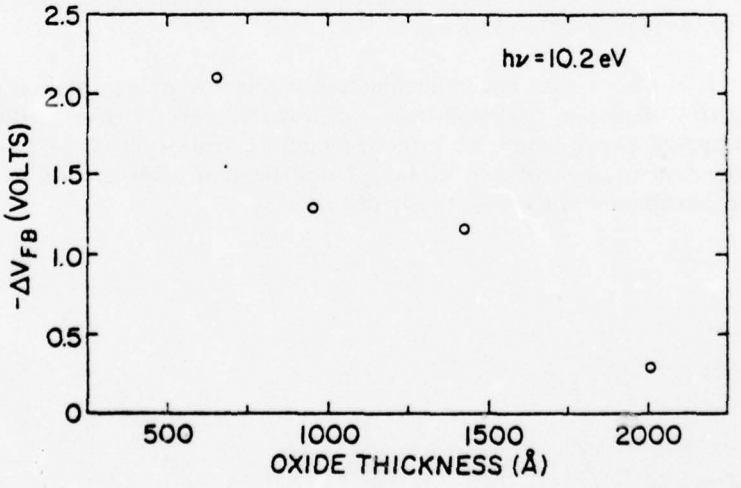

Fig. 4 The average flat-band voltage shift as a function of oxide thickness under equal illumination conditions with 10.2 eV photons for 0.5 min. The negative voltage applied to the aluminum was the equivalent of an average field in the oxide of 1×10^6 V/cm. The current through the oxide was 5×10^{-10} amp. The voltage shifts were divided by the oxide thickness to reflect the equivalent shift for a 1000 Å oxide.

ELECTRON TRAPPING AND DETRAPPING CHARACTERISTICS OF ARSENIC IMPLANTED SiO_2 LAYERS*

R. F. DeKeersmaecker and D. J. DiMaria

IBM Thomas J. Watson Research Center Yorktown Heights, NY 10598

Typed by: Kathlyn C. Murray

Abstract: The electron trapping properties of As^+ ion implanted thermally grown SiO_2 layers incorporated into MOS (metal-silicon dioxide-silicon) structures have been studied using avalanche injection charging and photocurrent-versus-voltage (photo I-V) measurements. After a $1x10^{13}$ As^+/cm^2 implant and a 1000°C anneal in N_2 for 30 min., a dominant trapping center with a capture cross section $\sigma_c \approx 1x10^{-15}$ cm^2 and a trap density $N_T \approx 6x10^{12}$ cm^{-2} is found independent of ion energy (10-100 keV), avalanche injection current ($5x10^{-11}-5x10^{-10}$ A), and oxide thickness (490-1410 Å). The dominant trap density is proportional to the ion fluence over our experimental range ($3x10^{12}-1x10^{14}$ As^+/cm^2). Minor trapping centers with σ_c ranging from 10^{-14} to $3x10^{-16}$ cm^{-2} have been measured.

The negative charge distribution centroid is shown to be proportional to the ion energy but does not depend on trapped charge density ($4x10^{11}-1x10^{13}$ cm^{-2}), ion fluence ($3x10^{12}-1x10^{14}$ cm^{-2}), injection mechanism (avalanche injection or internal photoemission) or oxide thickness (490–1410 Å).

It is shown that under illumination within the proper photon energy range, the trapped negative charge is removed from the trapping centers in a homogeneous way. From the detrapping experiments, an effective photoionization cross section is determined, which is defined as the convolution of the photoionization cross section with the optically accessible trap distribution in the energy gap of the SiO_2.

* This research was supported by the Defense Advanced Research Projects Agency and monitored by the Deputy for Electronic Technology, RADC, under Contract F19628-76-C-0249.

I. INTRODUCTION

Besides introducing surface states at the Si-SiO_2 interface of metal-silicon dioxide-silicon (MOS) structures [1,2], ion implantation has been known for some time to introduce electron trapping levels in the SiO_2 layer [3-9].

It has been proposed that this phenomenon can be used to harden MOS devices which have to operate in an ionizing radiation ambient [10,11]. In device applications, however, where ion implantation through an SiO_2 layer has often become a routine production step [12], the electron trapping phenomenon is expected to dramatically decrease the device lifetime in certain applications due to hot electron injection. The avalanche injection procedure as used in this paper, allows us to force a constant current through the oxide layer, charging even neutral trapping centers undetectable by conventional capacitance-versus-voltage (C-V) measurements which simultaneously makes accurate lifetime predictions and trapping parameter determinations feasible.

The electrical activity of impurities in the SiO_2 layer of MOS structures is only partially understood [13]. Since ion implantation has become available as a unique and controllable way of introducing impurities into the SiO_2 layer, our understanding of the electrical activity of those impurities is expected to improve quickly. In this paper, we investigate in detail the properties of SiO_2 layers implanted with As^+ ions which are a standard dopant in modern silicon technology.

The combination of electrical and photoelectric measurements as applied in this paper opens widespread possibilities for the investigation, with an unprecedented sensitivity, of defects in insulators not only related to ion implantation, but also to other fabrication techniques allowing energetic radiation to impinge upon the oxide.

As the annealing treatment after implantation becomes more effective, it is expected that the effects related to damage will disappear and that there will be an increasing correlation

between the nature of the implanted ions and the remnant trapping characteristics. The relation between the charge distribution centroid and the ion distribution centroid [9] as discussed here is evidence for this correlation.

The ion implanted As related trapping centers are shown to liberate their charge upon illumination with the proper photon energies and this photodetrapping phenomenon is also investigated in detail.

II. EXPERIMENTAL

A. Sample Fabrication

The samples used were 0.1 - 0.2 Ωcm p-type <100> silicon wafers. After thermal oxidation in a "dry" oxygen ambient to thicknesses ranging from 490 to 1440 Å (determined by ellipsometry), the wafers were given the As^+ implantation at room temperature with fluences ranging from $3x10^{12}$ cm^{-2} to $1x10^{14}$ cm^{-2} and ion energies from 10 keV up to 100 keV. Then all wafers were cleaned using the modified Huang procedure without the HF [14] and annealed in nitrogen at 1000°C for 30 min. unless otherwise specified. Using a shadow mask, thin (120-150 Å) circular aluminum electrodes with an area of 0.0052 cm^2 were deposited from an rf heated crucible at a pressure of 10^{-6} torr to form MOS capacitors. The semi-transparent metal electrodes were used to permit excitation of photocurrents from both the silicon and the aluminum contacts. The exact aluminum thickness was determined from a white light transmission measurement through aluminum deposited on quartz plates concurrently with the wafers.

Finally, all MOS devices were given a post-metallization annealing treatment at 400°C in forming gas (N_2/H_2 mixture) for 20 min. to reduce the surface states density.

B. Measurement of Trapping Properties

Avalanche injection [15,16] from the silicon substrate driven into deep depletion was used to inject electrons into the SiO_2 layer. Using an automated feedback circuit from the electrometer, the amplitude of a 50 kHz ramp wave was continuously adjusted in order to keep the average dc injection current constant at a preset level between 3×10^{-11} A and 5×10^{-10} A. The current was periodically interrupted to sense the flat-band voltage shifts which occur as some of the injected electrons are captured in the oxide. These flat-band voltage readings with the corresponding time readings were stored in a portable computer with an active workspace of 64 kbytes (IBM model 5100).

In the absence of detrapping, we can use first-order kinetics as treated by Ning and Yu [17] to derive the trapping parameters from the observed evolution of flat-band voltage shift in time at a constant avalanche injection current density j [18]:

$$\Delta V_{FB}(t) = eN_{eff}\,(L/\varepsilon)\,[1-\exp(-\sigma_c j\, t/e)] \tag{1}$$

where e is the electron charge, L is the oxide thickness, ε is the low frequency dielectric constant of SiO_2, σ_c is the capture cross section of the oxide traps and N_{eff} is their effective density defined by:

$$N_{eff} = (\bar{x}/L)\, N_T, \tag{2}$$

where $\bar{x}$ is the centroid of the trapped charge distribution as measured for the Al-SiO_2 interface, and N_T is the total density of available trapping sites $N_t(x)$ integrated over the oxide thickness:

$$N_T = \int_0^L N_t(x)\, dx\,. \tag{3}$$

If more than one trapping center is present, the actual shift $\Delta V_{FB}(t)$ will be the summation of the individual contributions of each center, characterized by its own capture cross section $\sigma_{c,i}$ and density $N_{T,i}$ [19].

C. Measurement of Trapped Charge and its Centroid

Photocurrent-versus-voltage (photo I-V) characteristics for MOS structures have been shown to be sensitive to the amount of trapped charge and its centroid in the insulator [20]. To generate photocurrents in our MOS structures, a 900 W xenon lamp was used in combination with a 500 mm grating monochromator (Bausch and Lomb). At positive (negative) gate bias a photon energy of 5(4.5) eV was used in order to excite electrons over the SiO_2-Si(Al) barrier. Room temperature current measurements were done in air with the remote head of a fast picoammeter (Keithley model 417) directly connected to the sample chamber fitted with a quartz window. Front contact to the MOS samples was made using 5 mil electrochemically polished tungsten probes. The gate voltage was automatically increased, usually in 1 V steps and both voltage and current readings were directly stored into a computer.

After bulk charge trapping the photo I-V curves are expected to shift in a parallel way along the voltage axis, at least at higher gate voltages, and the shifts were shown to depend on the charge location for a given density [20]. The following relations are obtained for the gate voltage shifts at a fixed photocurrent level:

$$\Delta V_g^- = V_{gb}^- - V_{ga}^- = (L-\bar{x})Q/\epsilon \tag{4a}$$

$$\Delta V_g^+ = V_{gb}^+ - V_{ga}^+ = -\bar{x}Q/\epsilon \tag{4b}$$

where the superscripts (+ or −) refer to the metal gate polarity, the subscripts a and b refer to the sample before and after charging respectively, and Q is the integral of the trapped charge density over the oxide thickness.

It has been shown previously that the flat-band voltage shift ΔV_{FB} and ΔV_g^+ are equal

for bulk trapped charge if there are no additional charges at the Si-SiO_2 interface [20,21]. While ΔV_{FB} tracks the field in the silicon, and is, therefore, sensitive to both bulk oxide charge and charges at the Si-SiO_2 interface, ΔV_g^+ is only determined by the field in the oxide, which is not sensitive to charges right at the Si-SiO_2 interface. A one-to-one correlation between ΔV_{FB} and ΔV_g^+ is, therefore, only possible if there is no interface charge.

By combining eqs. 4a and 4b, the following expressions are obtained for the trapped charge density Q and the centroid $\bar{x}$ of its distribution:

$$Q = (\epsilon/L)(\Delta V_g^- - \Delta V_g^+) \tag{5}$$

$$\bar{x} = L\,[1 - (\Delta V_g^-/\Delta V_g^+)]^{-1}. \tag{6}$$

One of the features of the photo I-V technique as developed by DiMaria [20] is that it uses continuous light, so that transient photoelectric effects in the substrate can be allowed to decay. The use of degenerate Si is, therefore, not mandatory and it becomes possible to do complementary high frequency (1 MHz) capacitance-voltage (C-V) measurements [22] on the same sample before and after a photocurrent-versus-voltage run to monitor perturbations of the charge distribution. Reproducibility checks on photo I-V data were also performed to ascertain that the charge distribution was only minimally perturbed.

In order to reduce perturbation effects (additional trapping or photodepopulation) the measurement times were kept as short as possible (usually 24 sec. illumination time) but long enough to allow phototransients to decay and the light intensities were occasionally reduced using metal screens to yield the lowest possible photocurrents still compatible with present noise levels (useful current range: 10^{-13} – 10^{-11} A). Under positive gate bias an auxiliary white light lamp was used to assist the build-up of the inversion layer. Dark currents, although usually very small, have been subtracted from the measured photocurrents before the data were stored.

D. Photodetrapping Measurements

After charging the traps in the oxide by avalanche injection from the Si or by internal photoemission from the Si or Al [23], the optical detrapping was studied at successively increasing photon energies using the same monochromator as described above. An electric shutter was used to control the time of illumination which was usually 5 min. The flat-band voltage shift resulting from this illumination was monitored using an automated set-up.

For optical measurements at temperatures below room temperature, a liquid nitrogen transfer system (Air Products) was used in connection with an optical cryostat. In order to characterize the detrapping phenomenon, the photon flux at the sample position had to be measured. For this purpose, a thermopile with a CaF_2 window was used in combination with a 13 Hz chopper (Bulova) and a lock-in amplifier (PAR model 124). A blank quartz disc simulated the presence of the sample chamber window.

III. ANALYSIS OF AVALANCHE INJECTION DATA

A. Ion Energy Dependence

Figure 1 shows the flat-band voltage shift variation as a function of time for samples implanted with varying ion energies. The faster charging at higher ion energies reflects the increasing penetration depth which also yields larger charge distribution centroids $\bar{x}$. The analysis described in Section II. B was applied to reduce the data using a computer program that is able to extract the parameters for two predominate trapping centers. The results for the capture cross sections and trap densities from the avalanche injection at 9×10^{-11} A of samples implanted at various ion energies are included in Table I.

To obtain N_T, data for the charge centroid $\bar{x}$ determined in Section IV had to be used. It was assumed here that the different trapping centers result in charge distributions with

identical centroids. This assumption is supported by experimental evidence, as will be discussed later.

From Table I, it is concluded that a major trapping center with a capture cross section $\sigma_c \approx 0.8 - 1.8 \times 10^{-15}$ cm^2 and a trap density $N_T \approx 5\text{-}6 \times 10^{12}$ cm^{-2} is measured at all energies and no obvious energy dependence is detected for these trap parameters.

B. Avalanche Injection Current Dependence

From eq. 1 it becomes clear that the charging time constant is given by

$$\tau = e/(\sigma_c j). \tag{7}$$

By changing the injection current density one is, therefore, able to scan a wide range of capture cross section magnitudes, since high current densities will bring low capture cross sections within the measurement time, and vice versa [19].

The trapping parameters for 2 samples resulting from avalanche injection at $I = 5 \times 10^{-10}$ A are included in Table I.

Using the magnitude of the capture cross section as a criterion, the measured trapping centers from Table I can be classified in 4 groups as done in Table II.

C. Ion Fluence Dependence

Increasing the implanted ion fluence is expected to increase the density of available trapping sites in the oxide. This was investigated by implanting a set of 3 wafers at an energy of 80 keV at increasing fluences of resp. 3×10^{12}, 10^{13} and 10^{14} As$^+$/cm^2. The results of the avalanche injection analysis are given in Table III.

It is seen that, if one considers the dominant trapping center with $\sigma_c \approx 1\text{-}2\ 10^{-15}$ cm^2, the trap density N_T scales fairly well with ion fluence.

D. Annealing Dependence

In order to determine whether a 1000°C treatment in N_2 for 30 min. is sufficient to saturate the annealing process, two wafers implanted with $1x10^{13}$ As^+/cm^2 at 60 keV received a different treatment, AS7E being annealed at 1000°C for 2 hours and AS7F at 1100°C for 30 min. The trapping parameters averaged over several runs for both wafers are summarized in Table IV.

It is interesting to note that a longer anneal at 1000°C does not affect the trapping parameters, but that a high temperature anneal (1100°C) reduced the trap density for center # 3 (see Table II). This reduced the trapping rate as compared to AS7D, implanted under the same conditions but annealed at 1000°C for 30 min.

E. Oxide Thickness Dependence

Wafer AS7M with a 490 Å thick SiO_2 layer was implanted with $1x10^{13}$ As^+/cm^2 at 20 keV. The trapping parameters were similar to those reported for MOS structures with 1400 Å thick SiO_2 layers.

IV. DISCUSSION OF TRAPPING PARAMETER RESULTS

(i) The capture cross section values which are detected in our experiments are indicative of electrically neutral trapping centers [24]. This is compatible with the approximately net neutral state of the virgin samples after implantation and annealing as indicated by C-V measurements. Since none of the centers are present in the control sample which went through the same fabrication steps except for the implantation, it is concluded that all the centers observed in our experiment are related to the ion implantation treatment.

(ii) Since the trap density for the major center # 3 (Table II) is not dependent upon implantation energy, it is concluded that the primary damage caused by

the implantation in the SiO_2 layer has been annealed out during the 1000°C treatment and that the trapping phenomena are closely related to the implanted ion species.

(iii) Since the capture cross sections which are detected are closely related to the injection current (eq. 7), not every trapping center mentioned in Table II will be charged by an avalanche injection run. If we assume that all 4 groups of trapping centers of Table II can be detected in a sample implanted at a given energy, the sum of the trap densities over all the centers has to be compared with the implantation fluence. Centers # 3 and 4 have actually been observed in the same run with trap density values close to the maximum of the range indicated in Table II. From the summation, it then follows that the total density of available traps can be larger than the density of implanted ions, indicating that every incoming ion is possibly able to generate more than one trapping site.

This observation is critically dependent upon the value for the charge centroid $\bar{x}$ used to calculate N_T from the quantity N_{eff} resulting from the data reduction (eq. 2). In our calculations we used a constant value for $\bar{x}$ for every implantation energy as determined in Section V. This procedure implicitly assumes that every trapping center has the same spatial distribution at a given ion energy. This assumption was experimentally verified as discussed below.

(iv) A similar implantation with 1×10^{13} Al^+/cm^2 at 30 keV into 730 Å thick SiO_2 layers followed by a 1050°C anneal was previously reported to exhibit trapping characteristics [7]. The dominant cross sections in that experiment were an order of magnitude lower ($1.26\ 10^{-16}$ cm^2 and $1.40\ 10^{-17}$ cm^2) which also indicates that the nature of the implanted ion strongly influences the trapping behavior. Moreover, in the case of the implanted Al^+ it was observed that the

trap density is proportional to the implant energy and is not independent of the energy as we have observed for As^+. This possibly indicates a different annealing behavior of the implantation induced damage for these cases.

(v) The initial trapping probability for electrons crossing the oxide is given by the product

$$\eta(0) = \sigma_c N_T. \tag{8}$$

Since N_T is proportional to the ion fluence Φ, it is useful to define a trapping probability per implanted ion $\eta(0)/\Phi$ which yields the number of trapped electrons per injected electron per ion present in the oxide. This ratio $\eta(0)/\Phi$ for the As^+ implantation related center # 3 is the highest encountered so far in an ion implanted oxide, which suggests concern for device applications of As^+ implanted oxide layers, even after a 1000°C anneal.

(vi) Field ionization of trapped charge was investigated on sample AS4X with a 1274 Å thick SiO_2 layer implanted at 60 keV with $1x10^{13}$ As^+/cm^2. After avalanche injection up to $\Delta V_{FB} \approx 8$ V, the sample was stressed with V_g = +40 V, which is approximately equal to the maximum oxide voltage drop during avalanche injection. Over a time period comparable to the injection interval, only 7.4% of the charge was lost.

V. ANALYSIS OF PHOTO I-V DATA

A. General Results

Figs. 2 and 3 show photocurrent measurements as a function of gate voltage for a typical sample with a positive and negative gate bias respectively. Since the effect of avalanche injection charging is to introduce a parallel shift in the photo I-V characteristics over a large voltage range, it is concluded that the major portion of the charge is located in the bulk of the

oxide, i.e. beyond the range of the potential maximum at the injecting interface [20]. From the shifts of the photo I-V characteristics, the centroid $\bar{x}$ and the areal density Q of the trapped charge can be calculated using eqs. 5 and 6. Flat-band voltage shifts after charging were very close to the photo I-V shift ΔV_g^+ for positive bias as expected for bulk oxide charging.

B. Centroids as a Function of Ion Energy.

Figure 4 shows the centroid $\bar{x}$ of the negative charge distribution after avalanche injection as a function of ion implantation energy [9]. Each point represents an average taken over several measurements. In the same figure, the solid line represents the theoretical values for the ion distribution centroids computed from the tables of Gibbons, Johnson, and Mylroie [25]. These theoretical centroid values differ from the tabulated values for the projected range R_p for two reasons:

(i) The density of thermal amorphous SiO_2 as used in our study is smaller than the density of single crystal SiO_2 as assumed in ref. 25 by a factor of 0.84.

(ii) The third moment (skewness) was included in our calculations. In our experiments, the skewness is positive, i.e. the profile has a trailing tail towards the Si-SiO_2 interface.

Figure 4 also includes the result of an independent determination of the ion distribution centroid using He^+ ion backscattering on a sample implanted with 10^{16} As^+/cm^2 at 100 keV [26]. As seen in the figure, there is an excellent agreement between the backscattering result for the ion distribution centroid and the photo I-V result for the trapped charge distribution centroid. Moreover, the photo I-V results closely follow the predicted values for the ion distribution centroid, especially at lower energies. The deviation at higher energies cannot be explained by penetration of As^+ ion into the Si substrate. It might be due to the fact that the

profile is more Gaussian than predicted by the theory, as also indicated by the results of ref. 26.

It is concluded from the results above, that the charge distribution is closely tracking the implanted ion distribution. This conclusion was also drawn for trapping related to implanted Al^+ and P^+ in SiO_2 after a 1000-1050°C anneal in N_2 for 30 min [9]. We believe that the high anneal temperatures used in our study allowed us to reduce the implantation related damage to a level where the nature of the implanted ion and its spatial distribution become the dominant features in the electron trapping phenomenon. Previous studies using a $1x10^{14}$ Al^+/cm^2 implantation at 20 keV without annealing [5] indicated that the trapped charge centroid differed from the ion distribution centroid, probably because the trapping occured mainly at displacement damage sites.

C. Further Centroid Studies

1. Dependence on trapped charged density.

During reproducibility measurements for the charge centroid determination, samples implanted at various energies were charged up to varying degrees of flat-band voltage shift. Within the small experimental error no dependence of the centroid on the charge level present in the oxide was found. Since during the avalanche injection the centers with the largest cross section will fill first, followed by those with smallercross sections, the latter observation means that the respective negative charge distributions associated with their corresponding trapping centers have very similar centroids. This result has previously been alluded to in Section IV (iii).

2. Detrapping experiments.

The photo I-V technique has also been used to ascertain that illumination with the proper energy removed trapped negative charge from the bulk of the oxide. This becomes clear e.g.

from figs. 5 and 6 where the photo I-V characteristics for sample AS4X after successive detrapping are shown respectively for positive and negative gate bias. The photo I-V shift for positive gate bias ΔV_g^+ is seen to track closely the decreasing ΔV_{FB}-value during photodetrapping, which eliminates the generation of compensating positive charge at the Si-SiO_2 interface as a possible explanation for the back-shift of the C-V characteristics during a detrapping experiment.

The detrapping experiments are performed with zero gate bias, in order to avoid injection from the contacts at photon energies greater than the SiO_2-Si(Al) energy barrier. The internal fields in the SiO_2 layer due to the trapped negative charge build an additional potential barrier against electron injection. But the same internal fields favor hole injection, especially from the Si valence band. Tunneling assisted hole injection into the SiO_2 and recombination with the trapped negative charge could then be viewed as an explanation for the 'detrapping' experiments, since at first sight this model would not be in conflict with the observed one-to one correspondence between ΔV_g^+ and ΔV_{FB}. The Si-SiO_2 interface with its high trapping probability for holes [27], however, is very likely to trap some of these injected holes, which would ultimately make ΔV_g^+ and ΔV_{FB} different. We, therefore, conclude that our experiments really involve the detrapping of negative charge.

It was also investigated whether the negative charge which is removed during photodetrapping is the same charge which was trapped during avalanche injection. Indeed, it could be conceived that in the uncharged sample compensating positive and negative charges are initially present and that, as the positive charge is being neutralized by injected electrons, an increasing amount of negative oxide charge emerges. In this case, the negative charge being removed during photodetrapping might <u>not</u> be the charge previously captured by the positive centers. The following experiment, however, weakens this model. An uncharged MOS structure on wafer AS4X was illuminated at 3.9 eV for $\approx$ 12 3/4 hrs. at Vg = +21 V without showing an appreciable detrapping of compensated negative charge, after it had been ascertained that

stressing at Vg = +21 V in the dark for ≈ 4 3/4 hrs. had no effect on the MOS structure.

Calculations for the charge centroid $\bar{x}$ after successive detrapping experiments show that the trapped negative charge is being removed in a homogeneous way, i.e. the centroid $\bar{x}$ was constant within the small experimental error. Since photodetrapping is favoring the depopulation of the centers with the highest photoionization cross sections σ_p, this would result in a varying charge centroid $\bar{x}$ if centers with different σ_p - values had different spatial distributions. The fact that $\bar{x}$ is essentially constant during photodepopulation is more support for our assumption that all trapping centers have approximately the same centroid.

3. Ion fluence dependence.

Table V summarizes the charge centroid values for three samples resp. implanted with As^+ fluences of $3x10^{12}$, $1x10^{13}$ and $1x10^{14}$ cm^{-2}, and all charged by avalanche injection at a current of $5x10^{-10}$ A. There is no correlation seen between the ion fluence and the charge centroid. Although the initial trapping probability given by eq. 8 is close to 10% for the major center in wafer AS7J implanted with $1x10^{14}$ As^+/cm^2, the centroid is not moving towards the Si-SiO_2 interface in that wafer.

4. Injection mechanism dependence.

Since, as discussed above, the initial trapping probability is so large for sample AS7J, we wanted to check whether the charge centroid would be dependent on the injecting interface, i.e. whether the injected electrons would be trapped closer to the interface from which they originate. As an injection mechanism from the Al electrode, we used internal photoemission under negative gate bias. This experiment was also important in the light of our study to be reported elsewhere [28], in which photoinjection and photodetrapping of an As^+ implanted SiO_2 layer is the basis for an MOS type non-volatile memory device. The result of our centroid measurements after photoinjection from the Al gate is included in Table V. Afte

charging wafer AS7J at Vg = −15 V up to $\Delta V_{FB} \approx 7$ V or at Vg = −30 V up to $\Delta V_{FB} \approx 16$ V, the charge centroids $\bar{x}$ as measured from the Al-SiO_2 interface were found to be 540 Å, which is very close to the value found after avalanche injection.

5. Oxide thickness dependence.

Sample AS7M with a 490 Å thick SiO_2 layer was implanted with $1x10^{13}$ As^+/cm^2 at 20 keV. Within experimental error, the charge centroid was equal to the one found in sample AS7B with a 1414 Å thick SiO_2 layer.

The observation that the centroid $\bar{x}$ is not smaller for the 490 Å thick SiO_2 layer than for the 1414 Å thick layer is evidence for the fact that even in the thin layer no implanted As is penetrating into the Si-substrate.

The charge centroid in sample AS7M was also verified to be very stable during photodetrapping experiments.

VI. PHOTODETRAPPING RESULTS

As was described in Section V. C. 2 the As^+ related trapping sites can be depopulated under illumination. By monitoring the flat-band voltage shift during detrapping we can deduce information on two important parameters, the photoionization cross section σ_p and the optical trap depth E_t, i.e. the energetic position of the trap level with respect to the bottom of the conduction band in the SiO_2.

A. Theory

Assuming first order kinetics and neglecting charge retrapping, the local depopulation of occupied traps under illumination is governed by the following equation:

$$\delta n_t\,(x,E,t)/\delta t = -F_p(x,\hbar\omega)\;\sigma_p(x,E,\hbar\omega)\;n_t(x,E,t) \qquad (9)$$

where $n_t(x,E,t)$ is the trapped electron concentration per unit energy (cm^{-3} eV^{-1}), $F_p(x,\hbar\omega)$ is the local photon flux in the SiO_2 layer ($cm^{-2}sec^{-1}$) and $\sigma_p(x,E,\hbar\omega)$ is the trap photoionization cross section (cm^2). The photon flux F_p is a function of both the photon energy $\hbar\omega$ and the position x in the SiO_2 layer measured from the Al-SiO_2 interface, due to the optical interference phenomenon [29]:

$$F_p(x,\hbar\omega) = F_p^0(\hbar\omega)\, F_p^1(x,\hbar\omega) \tag{10}$$

where $F_p^0(\hbar\omega)$ is the intensity spectrum for the lamp and $F_p^1(x,\hbar\omega)$ is the standing wave pattern in the oxide layer at photon energy $\hbar\omega$.

The photoionization cross section σ_p is a function of the trap energy level E in the SiO_2 band gap (E=0 and E_g at the top of the SiO_2 valence band and the bottom of the conduction band, respectively) and of the photon energy $\hbar\omega$ since it includes the transition probability to a final state $E+\hbar\omega$, and may be position dependent through a position dependent electric field due to the presence of charge in the SiO_2 layer. The field dependence of σ_p is neglected in our analysis.

Integrating eq. 9 over the oxide thickness and over the SiO_2 energy gap, therefore, yields:

$$d/dt\left[\int_0^L \int_0^{E_g} n_t(x,E,t)\,dE\,dx\right] = -\int_0^L \int_0^{E_g} F_p(x,\hbar\omega)\, \sigma_p(E,\hbar\omega)\, n_t(x,E,t)\,dE\,dx. \tag{11}$$

The integral on the left hand side of eq. 11 is the absolute value of total trapped charge Q (cm^{-2}) present in the SiO_2 layer.

At a particular photon energy ($\hbar\omega$), only centers between $E=E_g-\hbar\omega$ and $E=E_g$ can be depopulated, if thermal broadening of the trapping levels and two-photon processes are disregarded. This is equivalent to setting:

$$F_p(x,\hbar\omega) = F_p^o(\hbar\omega)\, F_p^1(x,\hbar\omega) \text{ for } E_g-\hbar\omega \le E \le E_g \tag{12a}$$

and

$$F_p(x,\hbar\omega) = 0 \text{ for } E < E_g - \hbar\omega. \tag{12b}$$

It is further assumed that the variables determining n_t are separable, i.e.

$$n_t(x,E,t) = n_t^{o}(t)\, n_t^{1}(E)\, n_t^{2}(x). \tag{13}$$

Physically this statement means that the charge distribution conserves its shape during discharging and, therefore, that the centroid $\bar{x}$ is constant in time, and further that all trapping centers have the same spatial distribution. Both assumptions are supported by centroid determinations from photo I-V data taken during a detrapping sequence as discussed in Section V.C.2.

After long discharging times, the charge centroid will ultimately be determined by the minimum in the light standing wave pattern. Since the illumination interval was small, however, compared to the discharing time constant, the interference effect could be disregarded.

The energetic and spatial trap distributions are normalized, i.e.

$$\int_o^{Eg} n_t^{1}(E)\, dE = 1 \tag{14a}$$

and

$$\int_o^{L} n_t^{2}(x)\, dx = 1. \tag{14b}$$

Equation 11 is rewritten as

$$-dQ/dt = -n_t^{o}(t) \left(\int_o^{L} F_p(x,\hbar\omega) n_t^{2}(x) dx\right)\left(\int_{E_g-\hbar\omega}^{E_g} \sigma_p(E,\hbar\omega) n_t^{1}(E) dE\right). \tag{15}$$

Multiplying both sides of eq. 15 by $\bar{x}/\varepsilon$ and using eq. 13 and 14 together with:

$$\Delta V_{FB}(t) = -(\bar{x}/\varepsilon)\int_o^{L}\int_o^{E_g} n_t(x,E,t) dE dx \tag{16}$$

finally yields:

$$d[\Delta V_{FB}(t)]/dt = -\Delta V_{FB}(t)\int_0^L F_p(x,\hbar\omega)n_t^2(x)dx\int_{E_g-\hbar\omega}^{E_g}\sigma_p(E,\hbar\omega)n_t^1(E)dE. \quad (17)$$

Equation 17 is abbreviated as

$$d[\Delta V_{FB}(t)]/dt = -\Delta V_{FB}(t)\ \chi(\hbar\omega)\ \Sigma(\hbar\omega) \quad (18)$$

where $\chi(\hbar\omega)$ is the convolution of the photon flux with the spatial distribution of the trapping centers and $\Sigma(\hbar\omega)$ is the convolution of the photoionization cross section with the optically accessible trap distribution over energy. The latter quantity will be viewed as an effective photoionization cross section.

The solution to eq. 18 is

$$\Delta V_{FB}(t) = \Delta V_{FB}(0)\exp[-\chi(\hbar\omega)\Sigma(\hbar\omega)t] \quad (19)$$

which can be approximated by

$$[\Delta V_{FB}(0)-\Delta V_{FB}(t)]/\Delta V_{FB}(0) = \chi(\hbar\omega)\Sigma(\hbar\omega)t \quad (20)$$

if

$$t << [\chi(\hbar\omega)\Sigma(\hbar\omega)]^{-1}. \quad (21)$$

Equation 20 is of experimental importance since the variation in flat-band voltage shift due to illumination for a period t can be measured, the quantity $\chi(\hbar\omega)$ can be calculated knowing the sample geometry and the photon energy used and, therefore, the effective photoionization cross section $\Sigma(\hbar\omega)$ can be determined.

B. Experiments

(i) In Fig. 7, the exponential variation of ΔV_{FB} with time is verified. It is seen that eq. 19 holds over a considerable period of time and moreover it follows

that for a measurement time of 5 min, eq. 21 is valid, which means that the approximation of eq. 20 applies for analyzing the measurements.

(ii) Figure 8 displays the effective photoionization cross section $\Sigma(\hbar\omega)$ measured at room temperature as a function of photon energy for wafer AS4X implanted with $1x10^{13}$ As^+/cm^2 at 60 keV.

Since $\Sigma(\hbar\omega)$ incorporates a convolution over all initial states (trapping centers) through $n_t^1(E)$, and over all final states through $\sigma_p(E,\hbar\omega)$ which includes the final state density $g(E+\hbar\omega)$ in the oxide conduction band, modeling of the $\Sigma(\hbar\omega)$ - structure is complicated. Experiments are under way, however, to shed more light on this problem.

VII. CONCLUSIONS

The electron trapping properties in well-annealed (usually at 1000°C in N_2 for 30 min.) As^+ implanted SiO_2 layers in MOS structures have been studied using avalanche injection and photocurrent-versus-voltage measurements.

After a $1x10^{13}$ As^+/cm^2 implant a dominant trapping center with a capture cross section $\sigma_c \approx 1x10^{-15}$ cm^2 and a trap density $N_T \approx 6x10^{12}$ cm^{-2} was found. The trap density was found to scale with the ion fluence. The ion energy, avalanche injection current density and oxide thickness did not influence the trapping parameters over the ranges used in our study.

Whereas prolonged annealing at 1000°C does not influence the trapping parameters, an anneal at 1100°C for 30 min. reduced the trap density from $\approx 6x10^{12}$ cm^{-2} to $1\text{-}2x10^{12}$ cm^{-2} in our study. The influence of the annealing temperature is presently under further investigation.

The centroid of the negative charge distribution as measured from the Al-SiO_2 interface was found to be proportional to the implantation energy. The trapped charge density, ion

fluence, injection mechanism and oxide thickness did not influence the charge centroid over the ranges used in our study.

Photodetrapping was shown to proceed in a homogeneous way, i.e. leaving the charge centroid unchanged as far as optical interference effects can be ruled out. From flat-band voltage shift measurements during photodetrapping at successively increasing photon energies, an effective photoionization cross section was determined, which is the convolution of the photoionization cross section with the optically accessible trap density in the energy gap of the SiO_2.

ACKNOWLEDGEMENTS

The authors would like to acknowledge stimulating discussions with D. R. Young; the sample preparation by the Silicon Process Studies Group; the thin Al metallization by E. D. Alley; and the experimental assistance of J. A. Calise and F. L. Pesavento.

REFERENCES

1. N. J. Chou and B. L. Crowder, J. Appl. Phys. 41, 1731 (1970).

2. W. Fahrner and A. Goetzberger in Ion Implantation in Semiconductors, Proc. II. Int. Conf. on Ion Implantation in Semiconductors, Garmisch-Partenkirchen, 1971, eds. I. Ruge and J. Graul (Springer, Berlin, 1971), p. 373.

3. L. I. Chen, K. A. Pickar, and S. M. Sze, Solid-St. Electron. 15, 979 (1972).

4. E. Harari and B. S. H. Royce, IEEE-NS 20(6), 288 (1973).

5. N. M. Johnson, W. C. Johnson, and M. A. Lampert, J. Appl. Phys. 46, 1216 (1975).

6. E. P. Jacobs and G. Dorda, Solid-St. Electron. 20, 367 (1977).

7. D. R. Young, D. J. DiMaria, and W. R. Hunter, J. Electron. Mat. 6, 569 (1977).

8. D. R. Young, D. J. DiMaria, W. R. Hunter, and C. M. Serrano, IBM J. Res. Develop. (to be published).

9. D. J. DiMaria, D. R. Young, R. F. DeKeersmaecker, W. R. Hunter, and C. M. Serrano, Electrochemical Society Fall Meeting, Atlanta, Georgia, 1977, Abstract No. 212 (to be published).

10. C. V. Perkins, K. G. Aubuchon, and H. G. Dill, IEEE-NS 15 (6), 176 (1968).

11. R. P. Donovan and M. Simons, J. Appl. Phys. 43, 2897 (1972).

12. G. Dearnaley, J. H. Freeman, R. S. Nelson, and J. Stephen, Ion Implantation (North-Holland, Amsterdam, 1973).

13. S. R. Butler and F. J. Feigl, Electrochemical Society Fall Meeting, Atlanta, Georgia 1977, Abstract No. 213 (unpublished).

14. E. A. Irene, J. Electrochem. Soc. 121, 1613 (1974).

15. E. H. Nicollian, A. Goetzberger, and C. N. Berglund, Appl. Phys. Lett. 15, 174 (1969).

16. E. H. Nicollian and C. N. Berglund, J. Appl. Phys. 41, 3052 (1970).

17. T. H. Ning and H. N. Yu, J. Appl. Phys. 45, 5373 (1974).

18. J. M. Aitken and D. R. Young, J. Appl. Phys. 47, 1196 (1976).

19. D. J. DiMaria, J. M. Aitken, and D. R. Young, J. Appl. Phys. 47, 2740 (1976).

20. D. J. DiMaria, J. Appl. Phys. 47, 4073 (1976).

21. R. J. Powell and C. N. Berglund, J. Appl. Phys. 42, 4390 (1971).

22. A. S. Grove, B. E. Deal, E. H. Snow, and C. T. Sah, Solid-St. Electron. 8, 145 (1965); A. S. Grove, Physics and Technology of Semiconductor Devices (Wiley, New York, 1967).

23. B. E. Deal, E. H. Snow, and C. A. Mead, J. Phys. Chem. Solids 27, 1873 (1966).

24. Let $\sigma_c = \pi r_c^2$ where r_c is the efective capture radius; r_c is close to the atomic dimensions for neutral centers.

25. J. F. Gibbons, W. S. Johnson, and S. W. Mylroie, Projected Range Statistics of Semiconductors and Related Materials, 2nd ed. (Halstead Press, Wiley, New York, 1975).

26. K. Tsukamoto, Y. Akasaka, and K. Horie, Japan. J. Appl. Phys. 16, 663 (1977).

27. D. J. DiMaria, Z. A. Weinberg, and J. M. Aitken, J. Appl. Phys. 48, 898 (1977) and references contained therein.

28. D. J. DiMaria, R. F. DeKeersmaecker, and D. R. Young (to be published).

29. D. J. DiMaria and P. C. Arnett, IBM J. Res. Develop. 21, 227 (1977).

TABLE I

Trapping parameters as a function of implant energy.

Sample	Ion energy (keV)	σ_{c1} (cm^2)	N_{T1} (cm^{-2})	σ_{c2} (cm^2)	N_{T2} (cm^{-2})
		Avalanche injection current $I = 9 \times 10^{-11}$ A			
AS7A	10	$1.2\ 10^{-15}$	$5.9\ 10^{12}$	$5.6\ 10^{-15}$	$1.4\ 10^{11}$
AS7B	20	$1.1\ 10^{-15}$	$5.1\ 10^{12}$	$1.1\ 10^{-14}$	$5.3\ 10^{10}$
AS7C	40	$1.0\ 10^{-15}$	$6.4\ 10^{12}$	$6.1\ 10^{-15}$	$3.6\ 10^{11}$
AS7D	60	$8.1\ 10^{-16}$	$6.1\ 10^{12}$	$5.6\ 10^{-15}$	$7.8\ 10^{11}$
AS7G	80	$1.7\ 10^{-15}$	$4.6\ 10^{12}$	$1.4\ 10^{-14}$	$5.6\ 10^{10}$
AS7H	100	$1.8\ 10^{-15}$	$5.6\ 10^{12}$	$1.6\ 10^{-14}$	$8.9\ 10^{10}$
		Avalanche injection current $I = 5 \times 10^{-10}$ A			
AS7A	10	$1.6\ 10^{-15}$	$3.9\ 10^{12}$	$2.2\ 10^{-16}$	$7.0\ 10^{12}$
AS7B	20	$1.2\ 10^{-15}$	$3.3\ 10^{12}$	$2.5\ 10^{-16}$	$5.8\ 10^{12}$

TABLE II

Summary of measured trapping centers after a $1x10^{13}$ As^+/cm^2 implant and a 1000°C anneal with their capture cross section and trap density.

Trapping Center #	σ_c (cm^2)	N_T (cm^{-2})
1	$1.1\text{-}1.6\ 10^{-14}$	$5.3\text{-}8.9\ 10^{10}$
2	$5.6\text{-}7.4\ 10^{-15}$	$1.4\text{-}7.8\ 10^{11}$
3	$0.7\text{-}1.8\ 10^{-15}$	$4.6\text{-}6.7\ 10^{12}$
4	$2.0\text{-}3.6\ 10^{-16}$	$1.8\text{-}7.0\ 10^{12}$

TABLE III

Trapping parameters as a function of As^+ ion fluence at a fixed energy of 80 keV.

Sample	Oxide Thickness (Å)	Ion Fluence (cm^{-2})	σ_{c1} (cm^2)	N_{T1} cm^{-2})	σ_{c2} (cm^2)	N_{T2} (cm^{-2})
		Avalanche injection current $I = 5x10^{-10}$ A				
AS7I	1423	$3x10^{12}$	$1.1\ 10^{-15}$	$2.0\ 10^{12}$	$1.8\ 10^{-16}$	$2.0\ 10^{12}$
AS7G	1415	$1x10^{13}$	$1.3\ 10^{-15}$	$5.7\ 10^{12}$	$6.5\ 10^{-15}$	$2.1\ 10^{11}$
		Avalanche injection current $I = 3x10^{-11}$ A				
AS7J	1405	$1x10^{14}$	$2.3\ 10^{-15}$	$4.3\ 10^{13}$	$4.0\ 10^{-14}$	$4.5\ 10^{10}$

TABLE IV

Trapping parameters as a function of annealing treatment after a $1x10^{13}$ As^+/cm^2 implant at 60 keV.

Wafer	Anneal	I (A)	σ_{c1} (cm^2)	N_{T1} (cm^{-2})	σ_{c2} (cm^2)	N_{T2} (cm^{-2})
AS7E	1000°C-2 hrs.	$5x10^{-10}$	$1.2\ 10^{-15}$	$7.6\ 10^{12}$	$4.3\ 10^{-15}$	$3.0\ 10^{11}$
		$9x10^{-11}$	$1.1\ 10^{-15}$	$8.3\ 10^{12}$	$7.6\ 10^{-15}$	$3.5\ 10^{11}$
AS7F	1100°C-30 min.	$5x10^{-10}$	$1.6\ 10^{-15}$	$2.0\ 10^{12}$	$3.7\ 10^{-16}$	$4.2\ 10^{12}$
		$9x10^{-11}$	$1.8\ 10^{-15}$	$1.0\ 10^{12}$	$4.7\ 10^{-16}$	$4.8\ 10^{12}$

TABLE V

Charge distribution centroid as a function of ion fluence. All samples were implanted at 80 keV.

Sample	Oxide thickness (Å)	As^+ fluence (cm^{-2})	Injection mechanism	Centroid (Å)
AS7I	1423	$3x10^{12}$	A	535
AS7G	1415	$1x10^{13}$	A	570
AS7J	1405	$1x10^{14}$	A	510
			P	540

A = avalanche injection from the Si substrate at I = $5x10^{-10}$ A.
P = photoinjection from the Al gate at 4.5 eV photon energy with V_G = -15 V and -30 V.

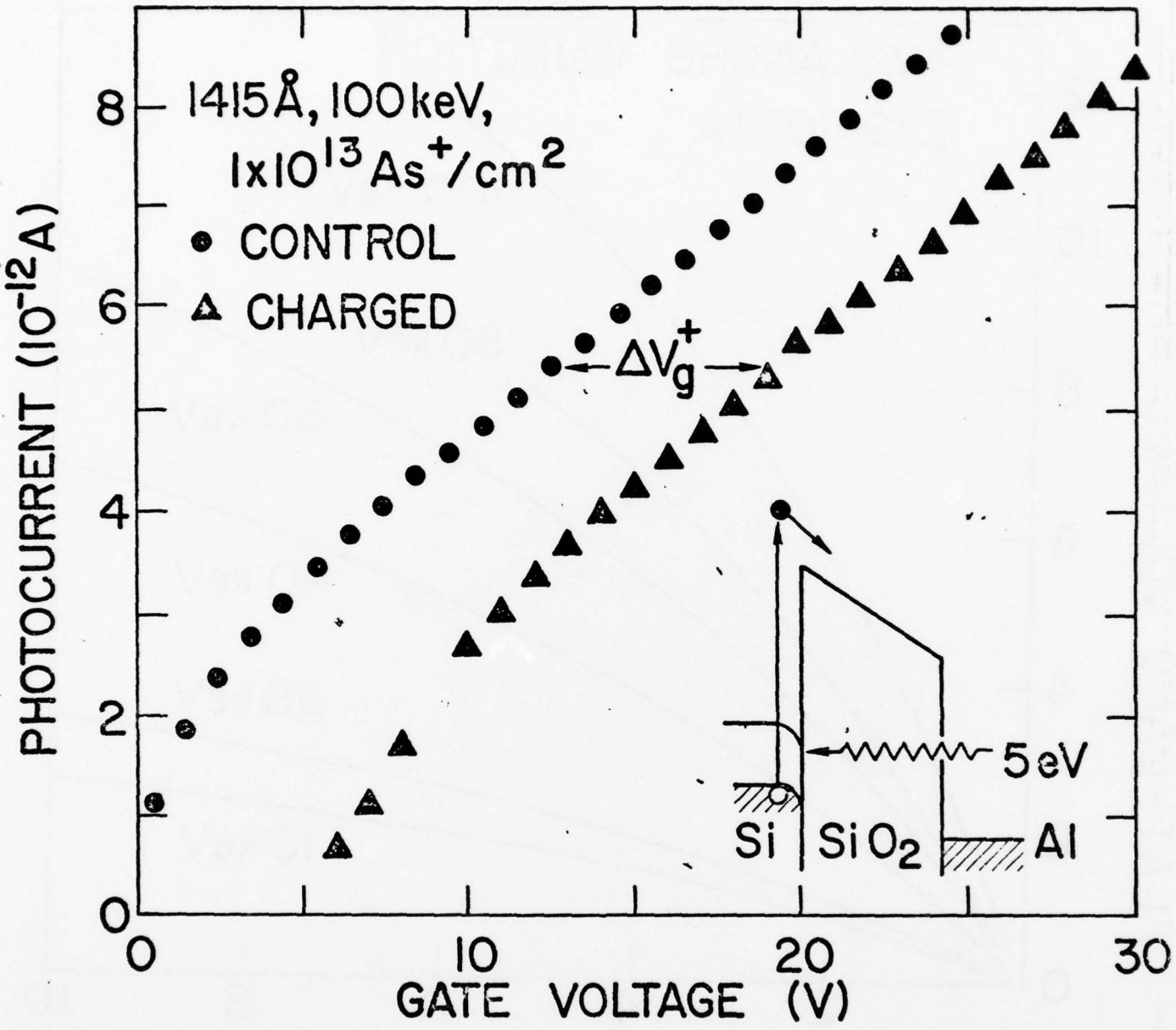

Fig. 2 Photocurrent as a function of applied gate voltage for positive bias before (solid circles) and after (solid triangles) partial charging of the As related traps by in situ avalanche injection. The sample was annealed in N_2 for 30 min. at 1000°C after implantation. The insert shows the energy band diagram for the uncharged MOS structure. Photon energy for the photo I-V measurements is 5 eV and the Si is the injecting electrode. $\Delta Vg^+ = 6.78 \pm 0.12$ V ; $\Delta V_{FB} = 6.3 \pm 0.3$ V.

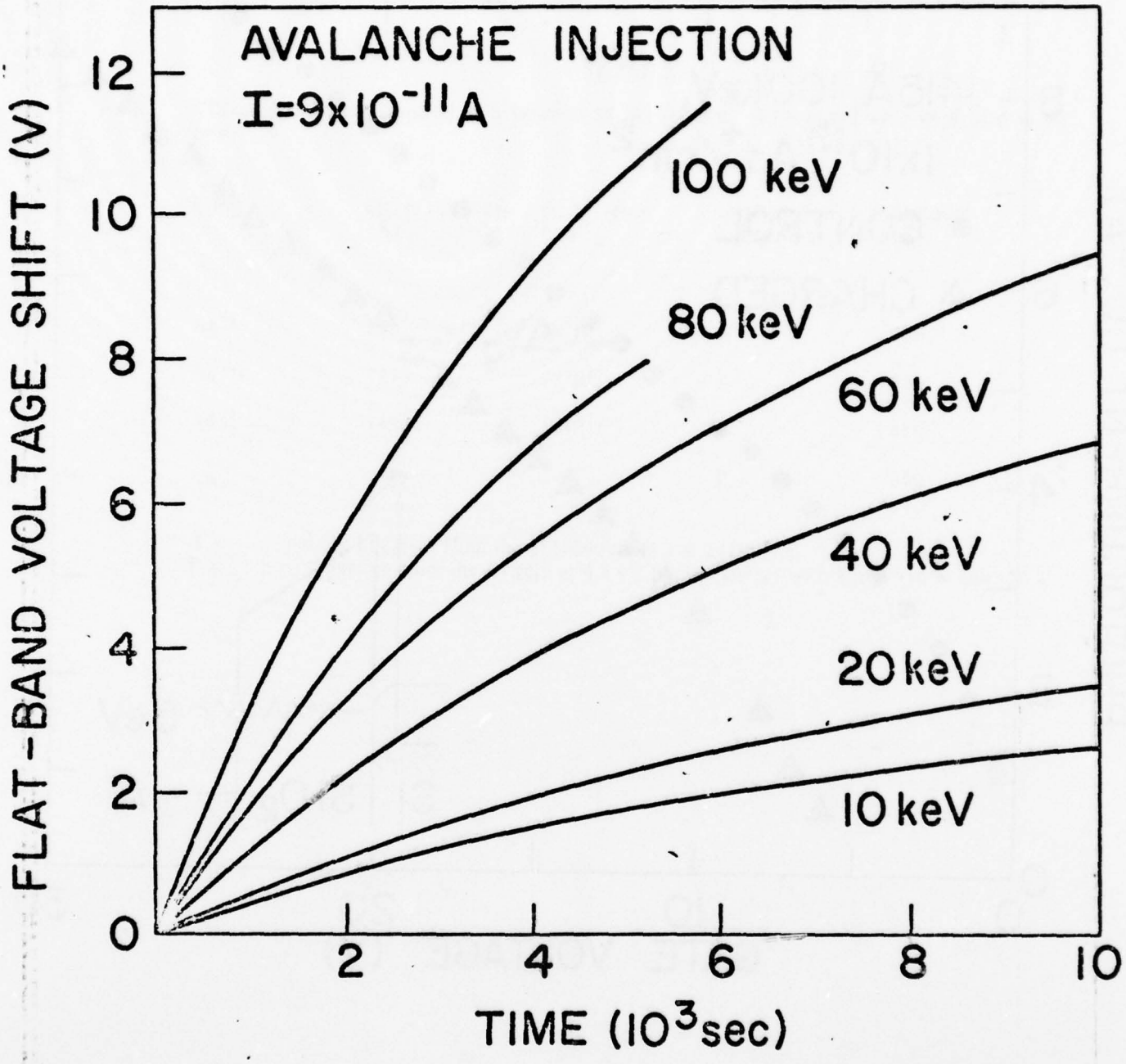

Fig. 1 Flat-band voltage shift as a function of time during avalanche injection at a current I = 9×10^{-11} A for various implantation energies. All samples were implanted with 1×10^{13} As^+/cm^2, have an average oxide thickness of 1410 Å and were annealed in N_2 for 30 min. at 1000°C.

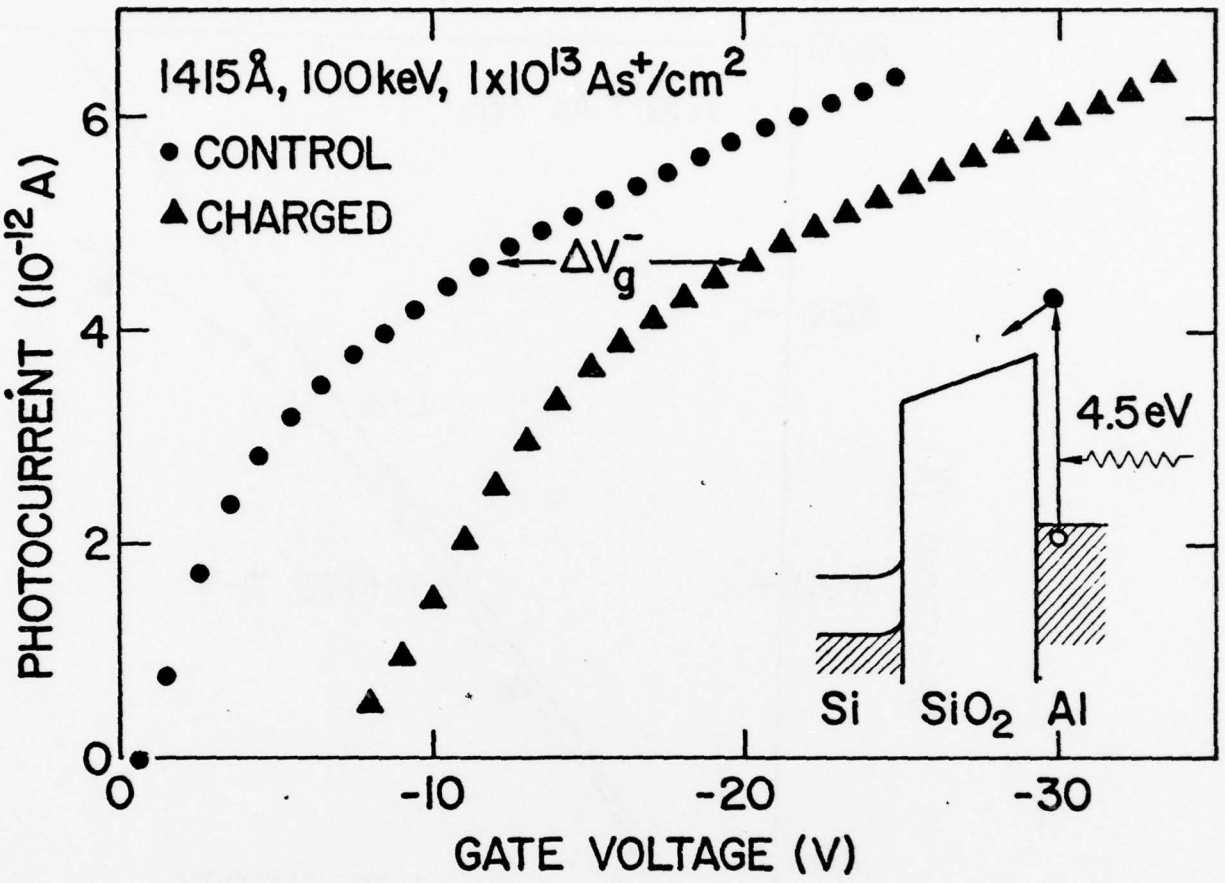

Fig. 3 Photocurrent as a function of applied gate voltage for negative bias before (solid circles) and after (solid triangles) partial charging of the As related traps by in situ avalanche injection. The sample was annealed in N_2 for 30 min. at 1000°C after implantation. The insert shows the energy band diagram for the uncharged MOS structure. Photon energy for the photo I-V measurements is 4.5 eV and the Al is the injecting electrode. $\Delta V_g^- = -8.05 \pm 0.11$ V; from ΔV_g^+ (fig. 2) and ΔV_g^- values $\bar{x} = 647$ Å and $Q/e = -2.2\ 10^{12}$ cm^{-2} are calculated (eqs. 5 and 6).

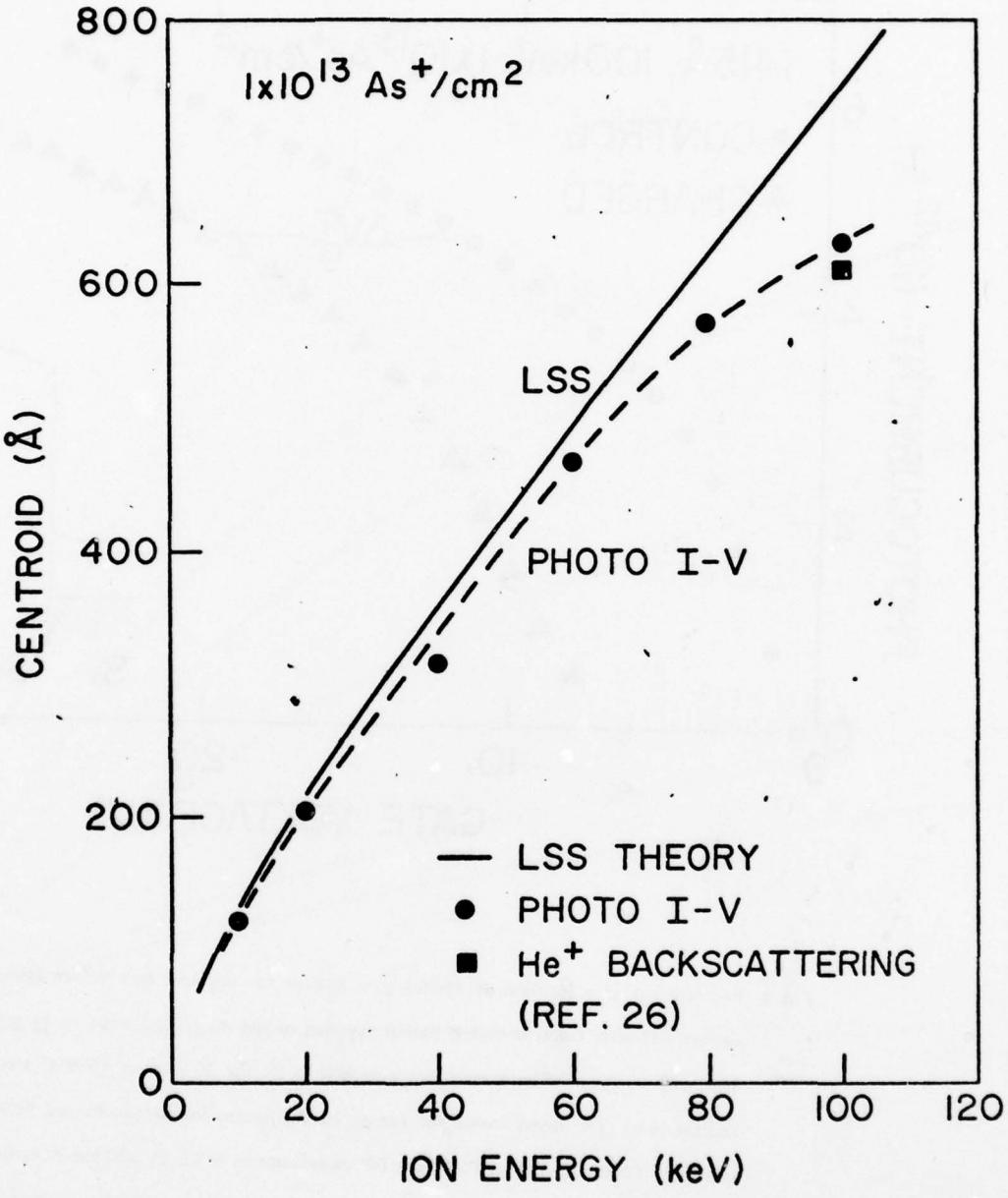

Fig. 4 Charge distribution centroid (from photo I-V data) and ion distribution centroid (from LSS theory including the third-moment correction) as a function of ion energy. The wafers had an average oxide thickness of 1410 Å, were implanted with 1×10^{13} As^+/cm^2 and annealed in N_2 for 30 min. at 1000°C. Also included is a He^+ backscattering result for a 1×10^{16} As^+/cm^2 implant into SiO_2 at 100 keV (ref. 26).

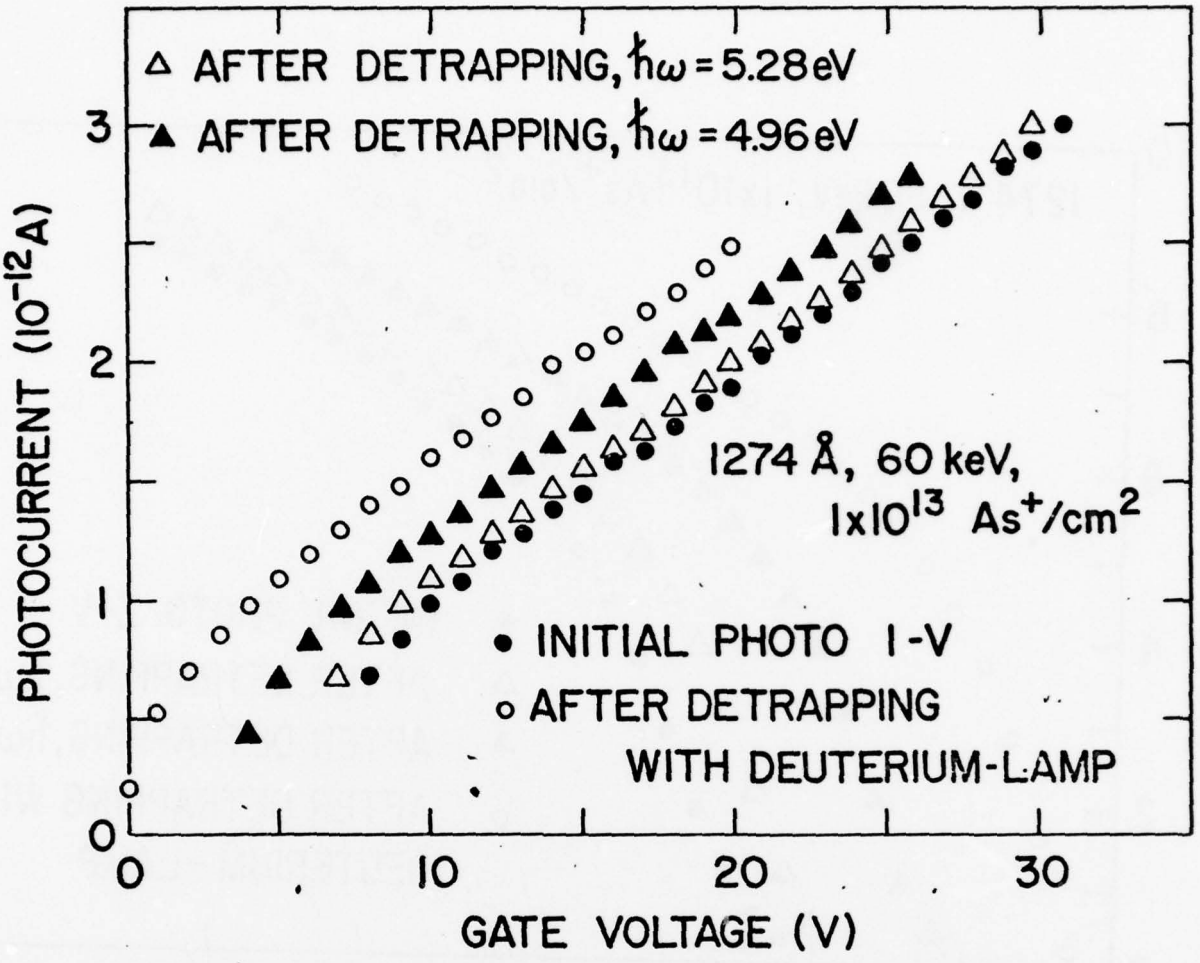

Fig. 5 Photocurrent as a function of applied gate voltage for positive bias for a sample initially charged by avalanche injection to ΔV_{FB} = +8.5 V, reduced to ΔV_{FB} = 7.8 V after a photoionization cross section measurement (see section VI), at successive stages of a detrapping sequence:

A. (solid circles) initial photo I-V.

B. (open triangles) after partial photodetrapping with V_g = 0 V at a photon energy of 5.28 eV for 298.5 min.; ΔV_{FB} = 6.7 V.

C. (solid triangles) after further photodetrapping with V_g = 0 V at a photon energy of 4.96 eV for 908.5 min.; ΔV_{FB} = 4.9 V.

D. (open circles) after further photodetrapping at V_g = −1 V with the whole spectrum of a deuterium-lamp (cut off with a filter at ≈ 5.5 eV) for 90 min.; ΔV_{FB} = 1.1 V.

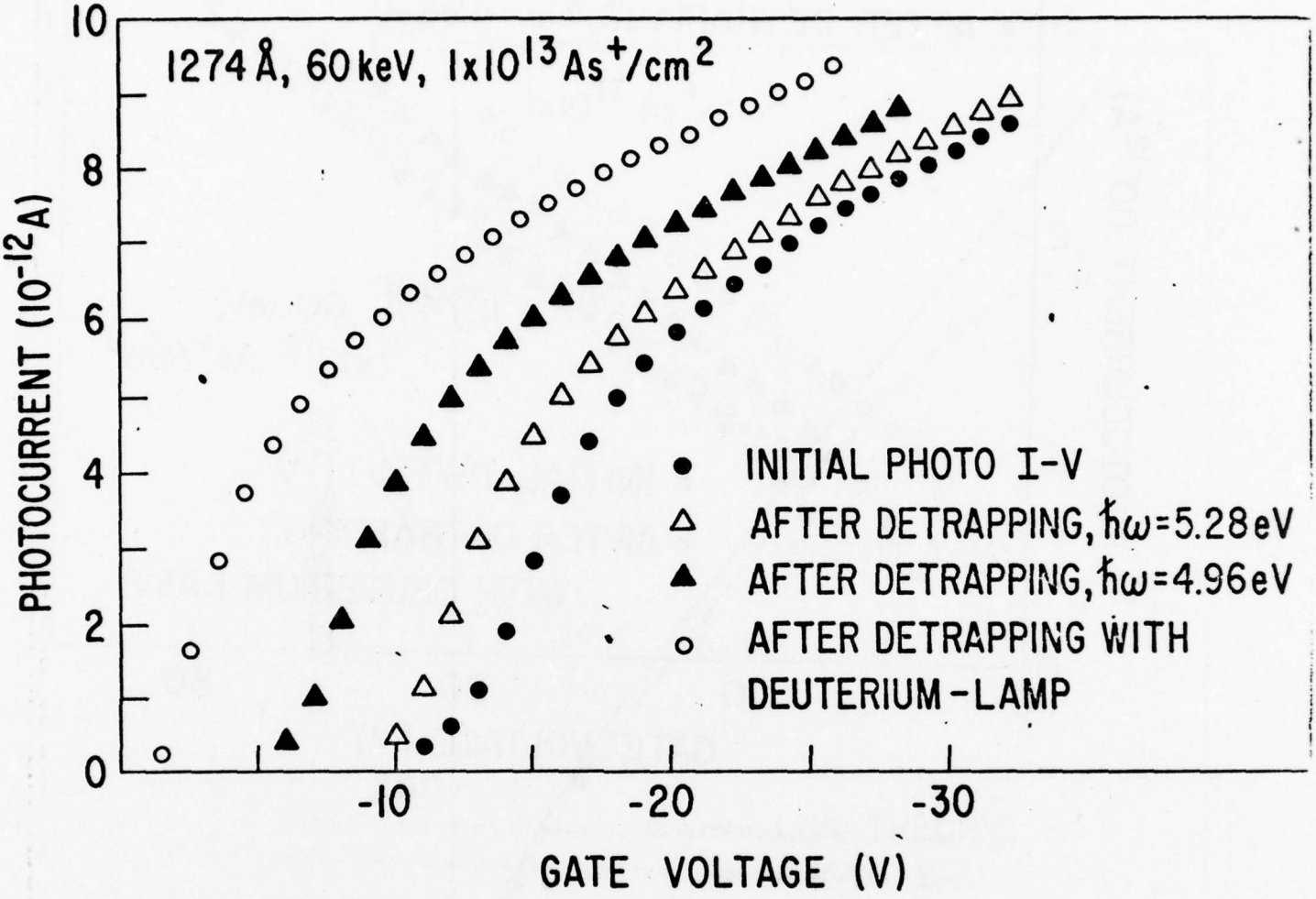

Fig. 6 Photocurrent as a function of applied gate voltage for negative bias for the same sample as in fig. 5.

The symbols have the same meaning as in Fig. 5.

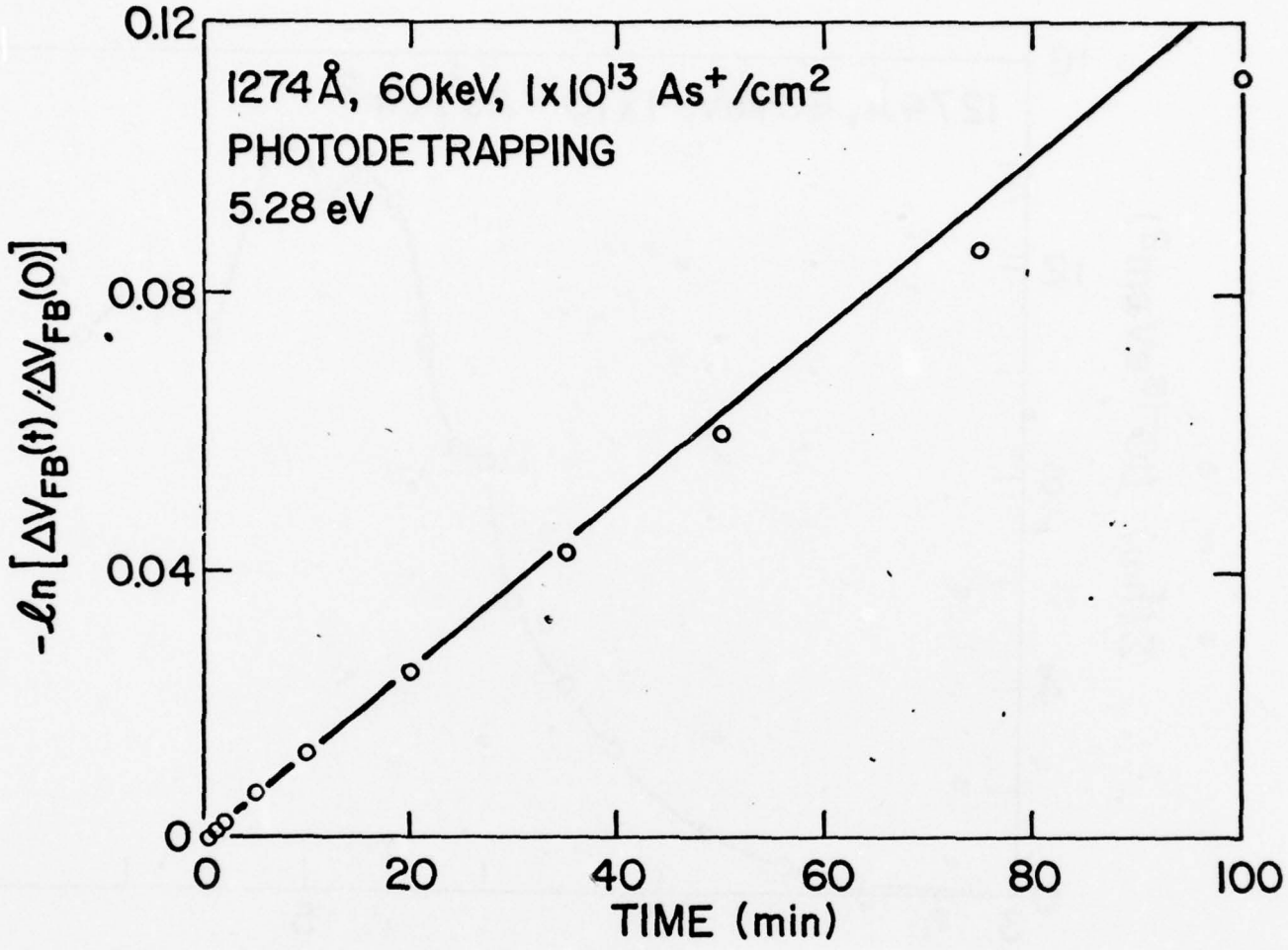

Fig. 7 Negative natural logarithm of the ratio $\Delta V_{FB}(t)/\Delta_{FB}(0)$ as a function of time during photodetrapping at $\hbar\omega$ = 5.28 eV from an initial flat-band voltage shift ΔV_{FB} = 7.5 V. The linear fit through the initial portion of the data is characteristic for exponential discharging with a time constant of 800 min.

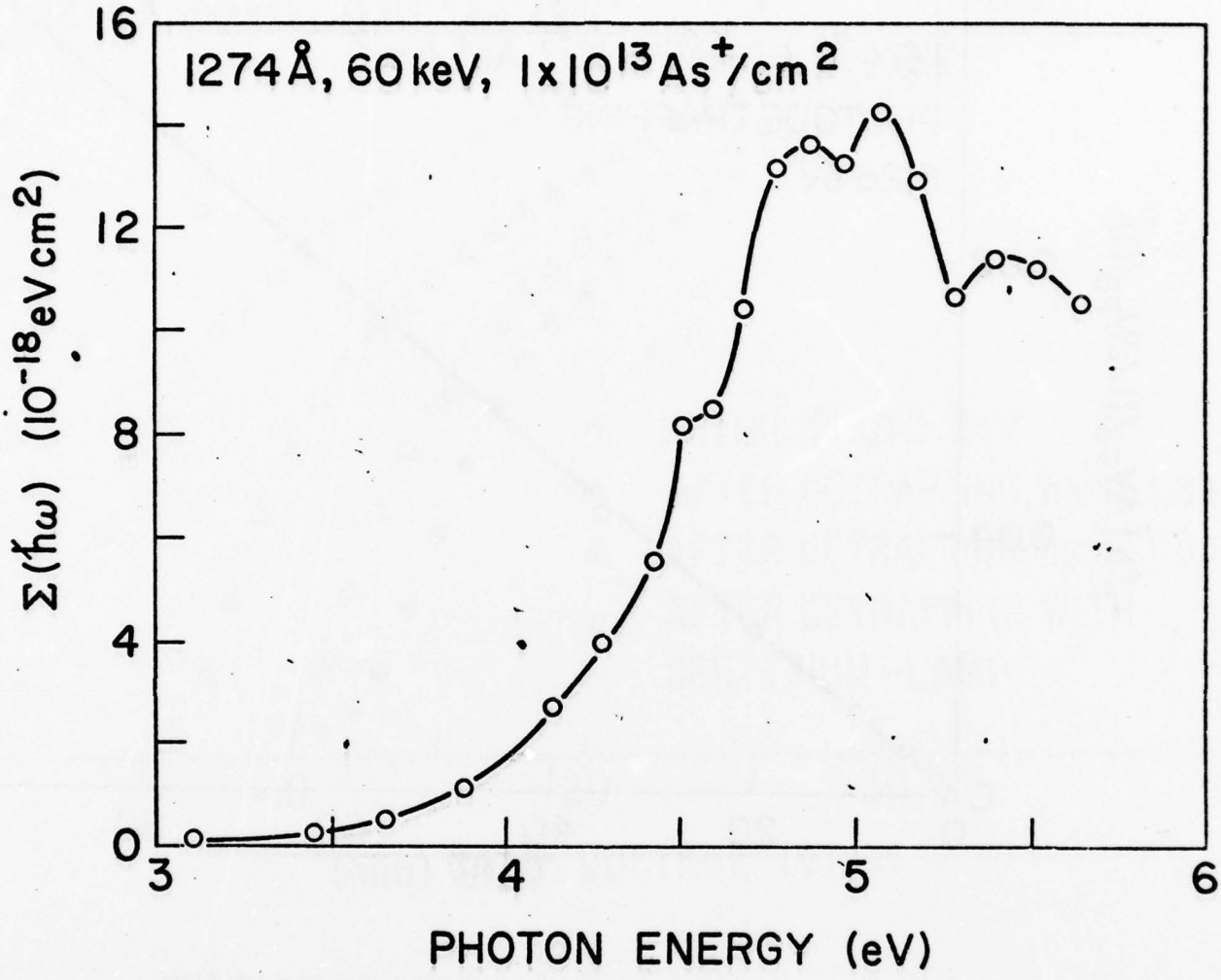

Fig. 8 Effective photoionization cross section $\Sigma(\hbar\omega) = \int_{E_g}^{E_g-\hbar\omega} \sigma_p(E,\hbar\omega)\, n_t^1\,(E)\, dE$, as a function of photon energy for a sample implanted with $1x10^{13}$ As^+/cm^2 at 60 keV, initially charged by avalanche injection at I = $9x10^{-10}$ A up to ΔV_{FB} (initial) = 10.65 V. At every photon energy, the MOS is illuminated for 5 min. with V_g = 0 V; ΔV_{FB} (final) = 9.82 V.

CENTROID LOCATION OF IMPLANTED IONS IN THE SiO_2 LAYER OF MOS STRUCTURES USING THE PHOTO I-V TECHNIQUE*

D. J. DiMaria, D. R. Young, R. F. DeKeersmaecker,
W. R. Hunter and C. M. Serrano

Technical Assistance of: J. C. Webber, E. D. Alley, F. L. Pesavento, J. A. Calise, and Silicon Process Studies Group

IBM Thomas J. Watson Research Center
Yorktown Heights, New York 10598

Typed by: Kathlyn C. Murray

Abstract: The centroids of various ions important in Si technology (Al, P, and As) implanted at energies from 5-100 keV and a fluence of $1x10^{13}$ cm^{-2} into 1300 - 1400 Å thick SiO_2 layers of metal-silicon dioxide-silicon (MOS) structures have been located by using the photo I-V technique. This technique indirectly senses trapped electrons on sites related to the implanted ions after charging by avalanche injection. A high temperature (1000°C in N_2 for 30 minutes) premetallization anneal was used in order to minimize trapping on atomic displacement damage sites which could give a different centroid than that of the ion distribution. Good agreement of the trapped electron centroid deduced by the photo I-V technique with LSS calculations of the ion centroid and with independent experimental determination of the ion centroid from profiles using secondary ion mass spectroscopy (SIMS) or He^+ ion backscattering was found in most cases. The photo I-V technique is shown to have distinct advantages over most techniques which directly measure the ion distribution or centroid like SIMS and He^+ ion backscattering because of its non-destructive nature, minimally perturbing effect, and extremely low detectability limit of 10^{11} charges/cm^2 or less. The empirical relationship observed by Chu, Crowder, Mayer, and Ziegler between the LSS normalized centroid ρ and the LSS normalized energy ϵ of $\rho = 2.7\epsilon$ has been shown for the first time to be valid for $\epsilon \leq .4$.

* This research was supported by the Defense Advanced Research Projects Agency and monitored by the Deputy for Electronic Technology, RADC, under Contract F19628-76-C-0249.

Ion implantation used in modern day processing is a convenient way to add impurities to Si or SiO_2. However, past attempts to study electron or hole trapping on implanted ions in SiO_2 has been unsuccessful due to large amounts of residual atomic displacement damage masking the presence of the ions [1]. By using a high temperature annealing treatment (1000°C in N_2 for 1/2 hour), electron trapping and detrapping on sites related to the implanted ions can be accomplished. Also a low ion fluence ($1x10^{13}$ ions/cm^2) was used to lower the electron capture probabilities of the traps (very few of the total number of injected electrons are captured) so that the centroid of the negative trapped charge would not depend on the injecting interface [1]. This communication shows that the centroids for this negative charge trapped on sites related to implanted Al, P, and As ions are identical to the centroids for the implanted ions. These centroids for trapped electrons were determined experimentally using the photo I-V technique [2-6] and compared to the ion location using secondary ion mass spectroscopy (SIMS) and He^+ ion backscattering. The experimental centroid locations are compared to those predicted from theoretical calculations based on the work of Lindhard, Scharff, and Schiøtt (LSS) using the tables of Gibbons, Johnson, and Mylroie [7]. The universal relationship between centroid and implantation energy in LSS normalized units of Chu et al. for implanted ions in amorphous insulators [8,9] is shown for the first time to be also valid at low energies for heavy ions (As) and at all energies for light ions (Al and P).

The thermal silicon dioxide layers were grown to a thickness of 1300-1400 Å on 0.1-0.2 Ωcm p-Si <100> substrates. The oxides were then implanted with either B, Al, P, or As at energies between 5–100 keV and a fluence of $1x10^{13}$ ions/cm^2. Metals and hydrocarbons were removed from the surface of the SiO_2 film using a cleaning procedure similar to that used by Irene [10] only with no HF. The samples were then annealed at 1000°C for 30 minutes in N_2, a thin Al gate electrode (100-160 Å) was deposited from an rf heated crucible, and finally a post-metallization, forming gas anneal at 400°C for 20 minutes was performed.

The SiO_2 layer was charged by avalanche injection [11,12] from the 0.1-0.2 Ωcm p-Si substrate using an automated set-up described previously [13]. High frequency capacitance-voltage (C-V) measurements were performed using a 1 MHz Boonton meter. Photo I-V measurements were performed using a 900 W xenon lamp and a Bausch and Lomb monochromator set for a 50 Å band pass [14] and a 5 eV (4.5 eV) photon energy for positive (negative) gate bias, respectively. Most of the photo I-V measurements were performed using an automated set-up by which the voltage bias was stepped in 1 V or 1/2 V intervals every minute. After capacitive current transients due to the voltage step had decayed to a negligible value, the 4.5 eV or 5 eV light was only allowed to fall on the thin metal electrode (using an automatic shutter) for a 24 second interval. In some cases, metal screens were used to reduce the light intensity and thereby reduce the photocurrent to values between 10^{-11} and 10^{-13} A to decrease perturbation effects (additional trapping or photodetrapping).

The virgin metal-silicon dioxide-silicon (MOS) samples were initially in an approximately net neutral state before charging. Prior to and after charging of the traps in the SiO_2 layer photocurrent as a function of gate voltage (photo I-V) was measured for both metal gate voltage polarities [2-6]. From these photo I-V characteristics, the centroid of the negative trapped charge was determined from the magnitude of the parallel voltage shifts between curves for a given polarity before and after charging according to the relationship $\bar{x} = L(1 - \Delta V_g^-/\Delta V_g^+)^{-1}$ where $\bar{x}$ is the centroid measured from the metal-SiO_2 interface, L is the oxide thickness, and ΔV_g^- and ΔV_g^+ are the photo I-V voltage shifts for negative and positive gate voltage bias, respectively [2-6].

C-V characteristics were recorded prior to and after each photo I-V sequence. C-V flat-band voltage shifts after charging were identical to the positive photo I-V shifts as expected for negative bulk oxide charging [2,15]. Perturbation effects due to additional charge trapping or photodetrapping while sensing the trapped charge location with the photo I-V technique were shown to be negligible from photo I-V and C-V reproducibility measurements

[2,4]. Displacement current effects were also negligible due to small electron capture probabilities [2,4] and small trapped electron photoionization probabilities. Background electron trapping of the oxide layer was shown to be negligible (when compared to samples implanted with Al, P, As) on non-implanted SiO_2 MOS structures which had otherwise undergone the same processing and avalanche charging conditions as the ion implanted samples. Charge trapping on sites related to implanted B could not be resolved from background oxide trapping and will not be discussed further. Details of capture cross sections, photoionization cross sections, trap densities, and annealing effects associated with the implanted ions will be reported in later publications.

Figures 1-3 (solid circles) show the centroid of the negative charge trapped on sites related to the implanted ions as a function of ion implantation energy for Al, P, and As. Each point represents an average over many samples charged to different levels in many cases. The solid lines representing the centroid of the ion distribution were computed from the tables of Gibbons, Johnson, and Mylroie [7]. Corrections for the density of thermal amorphous SiO_2 as compared to the density of single crystal SiO_2 (density ratio .84) used in the tables were made. Also the calculated centroids take into account corrections due to the third-moment ratios listed in the tables. These corrections are formed by joining two half Gaussian profiles with different half widths. For the ions and implantation energies used here, the Gaussian distribution with the smaller half width is closer to the Al-SiO_2 interface. The open circles in Figs. 1-3 represent independent experimental determinations of the centroids of the ion distributions using SIMS (Figs. 1-2) or He^+ ion backscattering [16] (Fig. 3) on samples implanted at higher fluences (except for Al) because of detectability limits associated with these techniques. As seen in these figures, there is good agreement between experiment and theory except for the 5 keV P and 100 keV As ions. The same general trend between the centroids of the negative trapped charge and the LSS calculations is seen for all ions; the experimental results are somewhat closer ($\lesssim$50 Å) to the Al-SiO_2 interface than theoretically predicted. The 100 keV As point is $\approx$ 125 Å closer to the Al-SiO_2 interface than the LSS calculations. This suggests

that the distribution of ions and therefore negative trapped charge is more Gaussian than predicted theoretically which is supported by the He^+ ion backscattering work of Tsukamoto et al. [16]. The LSS theoretical value for the centroid of a Gaussian distribution (no third moment correction included) is 562 Å for 100 keV As which is closer to the experimental points in Fig. 3. The negative trapped charge centroid for the 5 keV P implanted samples clearly is not the same as that for the ion distribution (see Fig. 2). Also this point was not reproducible on different batches of samples fabricated under supposedly identical conditions months apart. This point will be deleted from discussions that follow.

Figure 4 shows the photo I-V centroid data of Figs. 1-3 plotted in dimensionless LSS normalized units [7-9]. LSS normalized units essentially scale the centroid-energy plots for mass and atomic number so that different ions can be plotted on one universal plot. For the SiO_2 substrate, we have used an average atomic number of 10 and an average atomic mass of 20 [8,9,17]. The solid line with a slope of 2.2 is a least squares fit of the data through the origin. The dashed line of slope 2.7 is the relationship found by Chu et al. for heavier ions at higher energies and fluences using He^+ ion backscattering techniques [8,9]. All the data presented here lie within the scatter and error bars of the data of Chu et al. (see Figs. 2 and 4 of references 8 and 9, respectively) where the two sets of data overlap at higher energies. The data of Chu et al. actually are for the projected ion range rather than the centroids, but these are essentially equivalent for the high energies and heavy ions they used (ion distribution is Gaussian to within their experimental error). The data presented in Fig. 4 for LSS normalized energies $\leq .4$ shows for the first time the validity in amorphous insulators of the 2.7 slope at very low implant energies.

The photo I-V technique has been used to show that centroids of implanted ion distributions can be determined from negative trapped charge on sites related to the implantation. Combining the photo I-V technique with successive oxide etch-back steps after charging where photo I-V data is obtained at each step to determine the total trapped charge left behind

or removed, one can profile the charge distribution and therefore the ion distribution. The non-destructive analog of this technique in semiconductors would be C-V profiling which measures the electrical activity of the diffused or implanted ions [18,19]. The lower detectability limit for sensing bulk trapped negative charge using the photo I-V is at least $1x10^{11}$ cm^{-2} which is very difficult if not impossible to obtain with other techniques like SIMS or He^+ ion backscattering which directly sense the implanted ions. In future experiments, this technique will be extended to other ions, energies, and fluences to increase the information on implanted ion-amorphous material interactions.

The authors wish to acknowledge the critical reading of this manuscript by B. L. Crowder and M. I. Nathan; the SIMS measurements of F. W. Anderson and J. C. Webber of the IBM East Fishkill, NY Facility; the sample preparation by C. M. Osburn, J. M. Blum, and the Silicon Process Studies Group; the thin Al metallization by E. D. Alley; and the experimental assistance of F. L. Pesavento and J. A. Calise.

REFERENCES

1. N. M. Johnson, W. C. Johnson, and M.A. Lampert, J. Appl. Phys. 46, 1216 (1975).
2. D. J. DiMaria, J. Appl. Phys. 47, 4073 (1976).
3. D. J. DiMaria, Z. A. Weinberg, J. M. Aitken, and D. R. Young, J. Electron. Mat. 6, 207 (1977).
4. D. J. DiMaria, Z. A. Weinberg, and J. M. Aitken, J. Appl. Phys. 48, 898 (1977).
5. J. M. Aitken, D. J. DiMaria, and D. R. Young, IEEE Trans. Nucl. Sci. NS-23, 1526 (1976).
6. D. J. DiMaria, J. Appl. Phys. (Dec. 1977).
7. J. F. Gibbons, W. S. Johnson, and S. W. Mylroie, Projected Range Statistics of Semiconductors and Related Materials, 2nd edition (Halstead Press, John Wiley and Sons, 1975).
8. W. K. Chu, B. L. Crowder, J. W. Mayer, and J. F. Ziegler, Appl. Phys. Lett. 11, 490 1973).
9. W. K. Chu, B. L. Crowder, J. W. Mayer, and J. F. Ziegler, in Ion Implantation in Semiconductors and Other Materials, edited by B. L. Crowder, (Plenum Press, New York, 1973), pp. 225-241.
10. E. A. Irene, J. Electrochem. Soc. 121, 1613 (1974).
11. E. H. Nicollian, A. Goetzberger, and C. N. Berglund, Appl. Phys. Lett. 15, 174 (1969).
12. E. H. Nicollian and C. N. Berglund, J. Appl. Phys. 41, 3052 (1970).
13. D. R. Young, D. J. DiMaria, W. R. Hunter, J. Electron. Mat. 6, 569 (1977).
14. D. J. DiMaria and P. C. Arnett, IBM J. Res. Develop. 21, 227 (1977).
15. R. J. Powell and C. N. Berglund, J. Appl. Phys. 42, 4390 (1971).
16. K. Tsukamoto, Y. Akasaka, and K. Horie, Japan. J. Appl. Phys. 16, 663 (1977).
17. H. E. Schiøtt, in Ion Implantation, edited by F. H. Eisen and L. T. Chadderton (Gordon and Breach, New York, 1971), p. 197.

18. W. van Gelder and E. H. Nicollian, J. Electrochem. Soc. 118, 138 (1971).

19. D. P. Kennedy, P. C. Murley, and W. Kleinfelder, IBM J. Res. Develop. 12, 339 (1968).

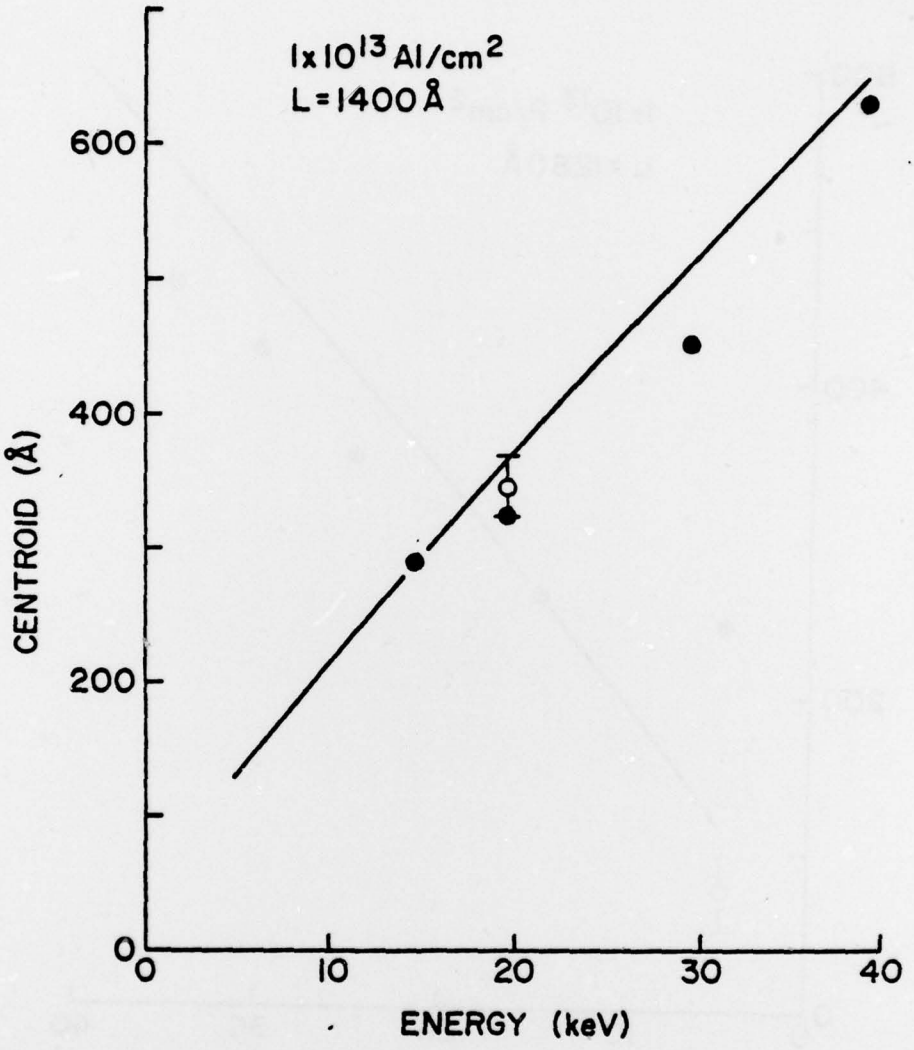

Fig. 1. Centroid as a function of implantation energy for an MOS structure with a 1400 Å thick SiO_2 layer implanted with a fluence of $1x10^{13}$ Al/cm^2. The solid points were experimentally determined for the negative charge trapped on sites related to the ion implantation using the photo I-V technique. The solid line is an LSS calculation using the table of Gibbons, Johnson, and Mylroie as described in the text for the ion distribution. The open circle was determined experimentally for the ion distribution using SIMS on a similar sample without the metal gate electrode.

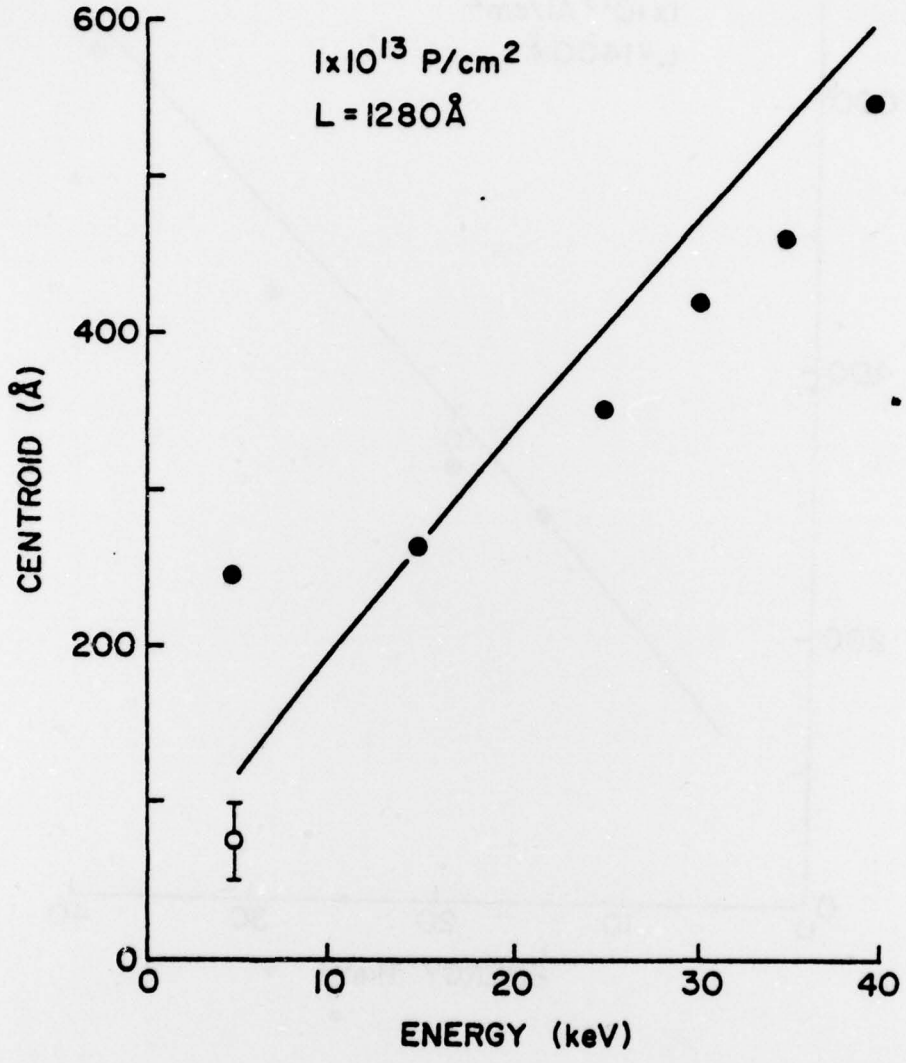

Fig. 2. Centroid as a function of implantation energy for an MOS structure with a 1280 Å thick SiO_2 layer implanted with a fluence of $1x10^{13}$ P/cm^2. The symbols have same meaning as in Fig. 1 except for the SIMS point (open circle) which was measured on a sample implanted with a $1x10^{14}$ P/cm^2 fluence without the metal gate electrode.

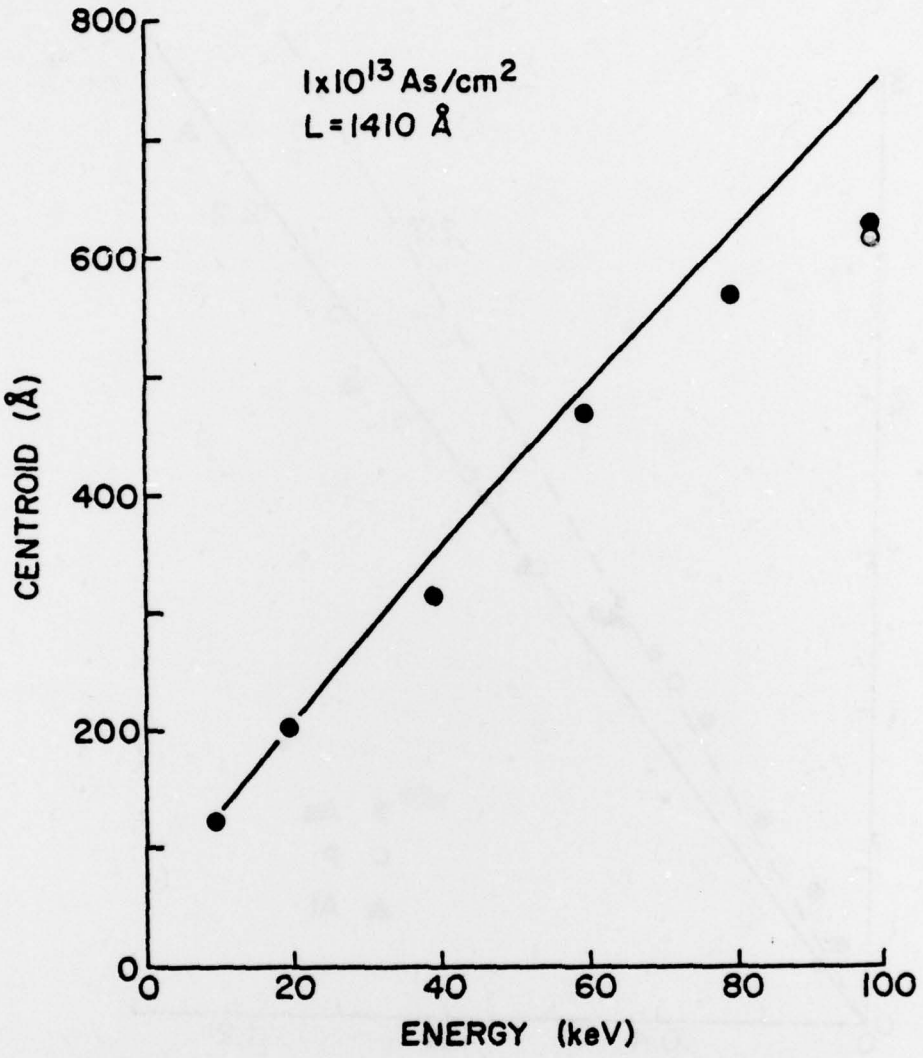

Fig. 3. Centroid as a function of implantation energy for an MOS structure with a 1410 Å thick SiO_2 layer implanted with a fluence of $1x10^{13}$ As/cm^2. The symbols have the same meaning as in Fig. 1 except for the open circle which represents an independent measurement by Tsukamoto et al. [16] of the centroid of the As ion distribution using He^+ ion backscattering techniques on a similar sample implanted with a fluence of $1x10^{16}$ As/cm^2 without the metal gate electrode.

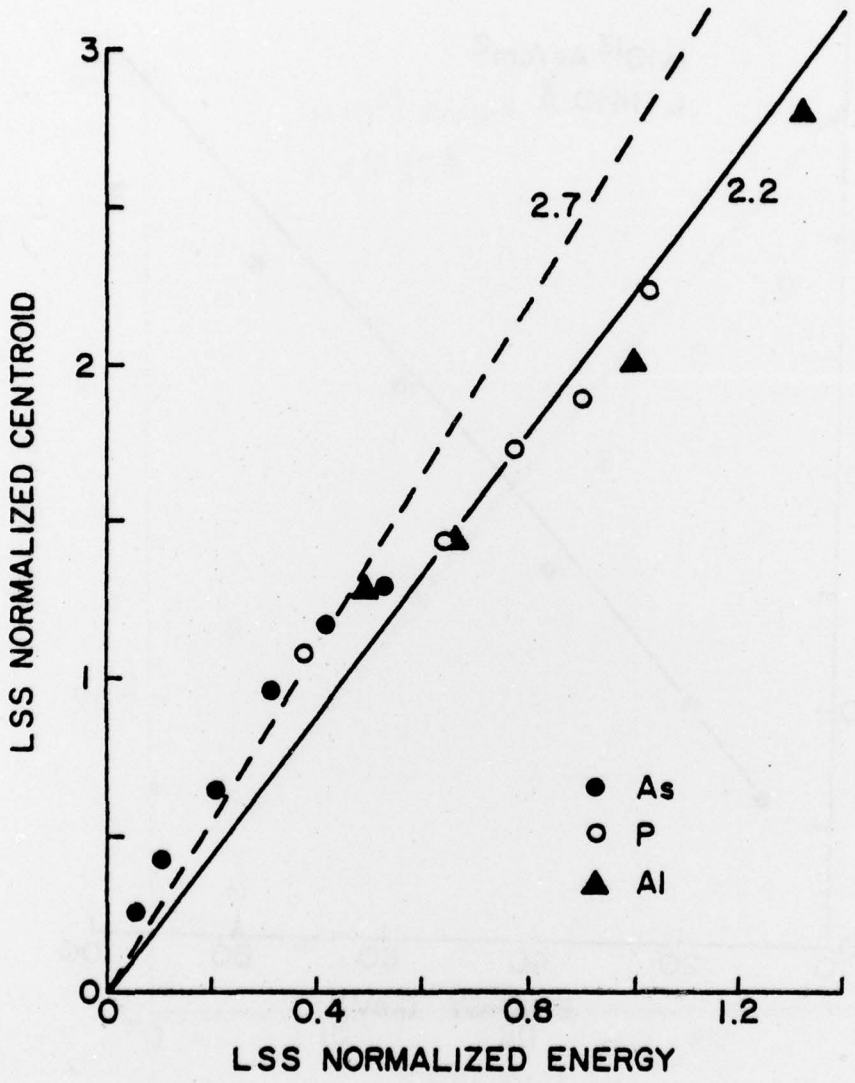

Fig. 4. LSS normalized centroid in dimensionless units as a function of LSS normalized energy in dimensionless units. The experimental photo I-V data of Figs. 1-3 has been used with the omission of the anomalous 5 keV P point in Fig. 2: ● - As, O - P, and ▲ - Al. The solid line is a least squares fit of the data through the origin and has a slope of 2.2. The dashed line with a slope of 2.7 is the empirical relationship deduced by Chu et al. [8,9].